

Petrochronological study of chloritoid schist from Medvednica Mountain (Zagorje Mid-Transdanubian zone, Croatia)

Ivan Mišur^{*1}, Dražen Balen², Urs Klötzli³, Mirko Belak¹, Hans-Joachim Massonne^{4,5}, Mihovil Brlek¹ and Vlatko Brčić¹

¹ Croatian Geological Survey, Department of Geology, Sachsova 2, HR-10000 Zagreb, Croatia (*corresponding author e-mail: imisur@hgi-cgs.hr)

² University of Zagreb, Faculty of Science, Department of Geology, Division of Mineralogy and Petrology, Horvatovac 95, HR-10000 Zagreb, Croatia

³ University of Vienna, Faculty of Earth Sciences, Geography and Astronomy, Department of Lithospheric Research, Josef-Holaubek-Platz 2 (UZA II), 1090 Wien, Austria

⁴ University of Stuttgart, Faculty of Chemistry, Pfaffenwaldring 55, 70569 Stuttgart, Germany

⁵ School of Earth Sciences, China University of Geosciences, Lumo Road 388, Wuhan, 430074, China

doi: 10.4154/gc.2023.02



Abstract

Article history:

Manuscript received April 20, 2021

Revised manuscript accepted December 12, 2022

Available online February 23, 2023

The metamorphic conditions and evolution of the Palaeozoic-Mesozoic metamorphic complex of Medvednica Mountain (Zagorje-Mid-Transdanubian zone, Croatia) are still a matter of debate. The results of the investigation of five samples of metapelitic schists with the mineral association of quartz, white mica and chlorite are presented. The studied schists are part of the continental margin of Adria and were metamorphosed under upper greenschist- to amphibolite-facies conditions. The focus of this study is a sample representing the highest metamorphic grade that additionally contains chloritoid blasts. Pressure-temperature pseudosection modelling together with classical geothermobarometric calculations yielded peak metamorphic conditions of 0.94 ± 0.05 GPa and 550 ± 20 °C for chloritoid schist. Monazite in-situ U-Th-total Pb electron microprobe dating indicates two metamorphic events at 167 ± 2 Ma and 143 ± 2 Ma, which are interpreted as the time of monazite growth during two distinct metamorphic phases. The formation of the chloritoid paragenesis is related to the older event (around 167 Ma) and linked with the Middle Jurassic subduction-accretion processes of Neotethys-derived ophiolitic lithologies. The younger metamorphic event (around 143 Ma) is related to the obduction of ophiolites onto the continental margin of Adria.

Keywords: Medvednica Mountain, Zagorje Mid-Transdanubian Zone, chloritoid, geothermobarometry, monazite

1. INTRODUCTION

The study is focused on the metasedimentary succession of the Palaeozoic-Mesozoic metamorphic complex (PMMC) of Medvednica Mountain (Mt.) north of the city of Zagreb. The investigated metasediments are part of the Jadar-Kopaonik thrust sheet (BASCH, 1983a,b; KARAMATA, 2006; SCHMID et al., 2008) (Fig. 1), which originated at the continental margin of the Adria microplate promontory and are located along the present day contact of the Tisia and Adria microplates (SCHMID et al., 2008; 2020, SCHEFER et al., 2010 and references therein). Between these microplates, the opening and extension of the Neotethys occurred from the Middle Triassic to the Middle Jurassic, during which time intra-oceanic subduction occurred (BABIĆ et al., 2002; PAMIĆ, 2002; KARAMATA, 2006; SCHMID et al., 2008; 2020; ŠEGVIĆ et al., 2014; 2020). This subduction was followed by an accretion process and the subsequent obduction of Neotethys crust resulting in the formation of ophiolites (West Vardar ophiolites sensu SCHMID et al., 2008; 2020, and references therein) at the continental margin of Adria (CMA). Geochemistry and mineralogy of metasediments usually provide valuable information on the nature of the protolith and its metamorphic evolution. Therefore, we conducted a petrochronological study on the metasedimentary succession of the PMMC to better understand its evolution. The study primarily focuses on a sample containing chloritoid as an index mineral of the highest metamorphic grade in metasediments on Medvednica Mt.

Chloritoid schists of Medvednica Mt. were earlier reported by VRAGOVIĆ & MAJER (1979a,b), who described the petrog-

raphy and presented the chemical whole-rock compositions of their samples but without stating either a stratigraphic correlation or position within the PMMC of Medvednica Mt. MIŠUR et al. (2013) presented petrographic and whole rock analyses of the chloritoid schist from the southeastern slopes of Medvednica Mt.

We aimed to distinguish metamorphic records in the chloritoid schist. All samples in this study were analysed by petrographic microscope, followed by whole-rock analyses, whereas further chemical analyses of minerals were only carried out on the chloritoid-bearing sample. This research considers the possibility that the investigated metasedimentary succession of the PMMC could have recorded polymetamorphic overprinting of the aforementioned complex; a prograde phase, developed during the Jurassic subduction and collision of Adria and Europe (i.e. Tisia) (LANPHERE et al., 1975; OKRUSCH et al., 1978; DIMOLAHITTE et al., 2001; SCHMID et al., 2008; 2020; ŠEGVIĆ et al., 2014; 2020; BELAK et al., 2022) and a subsequent retrograde phase in the Early Cretaceous (110 – 125 Ma) related to ophiolite obduction onto the CMA during the final stage of ocean closure (VAN GELDER et al., 2015; BELAK et al., 2022).

2. GEOLOGICAL SETTING

The Middle Triassic opening of the Neotethys ocean was followed by intermediate and basic volcanism (PAMIĆ, 1984; SCHMID et al., 2008; VAN GELDER et al., 2015; SLOVENEC et al., 2020 and references therein). The passive continental margin of eastern Adria was formed simultaneously and is characterised mainly by siliciclastic and carbonate sedimentation

(PAMIĆ, 1984; SCHMID et al., 2008; VAN GELDER et al., 2015). During the late Middle Jurassic, intra-oceanic subduction in the Neotethys realm resulted in the formation of an accretionary wedge and thrusting of ophiolitic units forming a mélange (BABIĆ et al., 2002; SCHMID et al., 2008, 2020; SLOVENEC et al., 2010; ŠEGVIĆ et al., 2014; VAN GELDER et al., 2015). Later on, during the Late Jurassic – Early Cretaceous, Jurassic ophiolite lithologies (i.e. Western Vardar sensu SCHMID et al., 2008; 2020) were obducted onto the CMA (PAMIĆ, 2002; BABIĆ et al., 2002; KARAMATA, 2006; SCHMID et al., 2008; 2020). These events influenced the subsequent geological setup of the central part of Medvednica Mt.

Medvednica Mt. is situated in an area where Dinaridic, Carpathian, and Alpine units came into contact (Fig. 1). This area is known as the Zagorje–Mid–Transdanubian Zone (ZMTZ after PAMIĆ & TOMLJENOVIC, 1998), which evolved during the Cretaceous–Palaeogene collision of the Adria microplate with the European margin (PAMIĆ, 2002; USTASZEWSKI et al., 2009; TOLJIĆ et al., 2013). The ZMTZ was the major regional shear zone in the Oligocene–Pliocene, where the northern tip of the Dinaridic units was rotated clockwise from a NW–SE to a NE–SW orientation (SCHMID et al., 2008; TOMLJENOVIC et al., 2008; USTASZEWSKI et al., 2008; VAN GELDER et al., 2015). The northern boundary of the ZMTZ is the Periadriatic transcurrent fault merging eastward into the Balaton line (FODOR et al., 1998; HAAS et al., 2000; TOMLJENOVIC et al., 2008; and reference therein). The southern border of the ZMTZ is the Zagreb–Zemplin lineament which forms the border to the Tisia-Dacia mega-

block (CSONTOS & NAGYMAROSY, 1998; FODOR et al., 1998; HAAS et al., 2000) (Fig. 1).

Medvednica Mt. is composed of exhumed Jurassic ophiolitic lithologies that were obducted onto the PMMC and covered by Cretaceous and Tertiary sediments (Fig. 2) (ŠIKIĆ et al., 1978; 1979; BASCH, 1983a,b; BABIĆ et al., 2002; JUDIK et al., 2004; LUGOVIĆ et al., 2006; TOMLJENOVIC et al., 2008; VAN GELDER et al., 2015). The PMMC consists of metasediments, which were originally shale, sandstone, limestone, and chert interstratified with basalt and tuff, and was affected by several deformation events (BELAK et al., 1995a,b; JUDIK et al., 2004; LUGOVIĆ et al., 2006; TOMLJENOVIC et al., 2008; VAN GELDER et al., 2015). According to TOMLJENOVIC et al. (2008), these events were: (1) the Aptian–Albian nappe stacking in the central–northern Dinarides, (2) Early Albian orogen-perpendicular shortening, (3) E–W shortening that took place after the Palaeocene; and (4) right-lateral N–S shearing that was interpreted to be related to the right-lateral shearing of the Sava zone during the Eocene–Oligocene (PAMIĆ & TOMLJENOVIC, 1998; TOMLJENOVIC, 2002; TOMLJENOVIC et al., 2008).

The metamorphic conditions of the PMMC were determined using the Kübler index (JUDIK et al., 2004), the chlorite empirical thermometer and vitrinite reflectance thermometry (LUGOVIĆ et al., 2006; JUDIK et al., 2008). The temperature range of metamorphism of the PMMC was 300–410 °C, obtained using the Kübler index method (JUDIK et al., 2004; 2008) and 300–350 °C by applying chlorite geothermometry in metabasites (LUGOVIĆ et al., 2006). VRAGOVIĆ & MAJER (1979b) assumed metamorphic P-T conditions for chloritoid schist up to

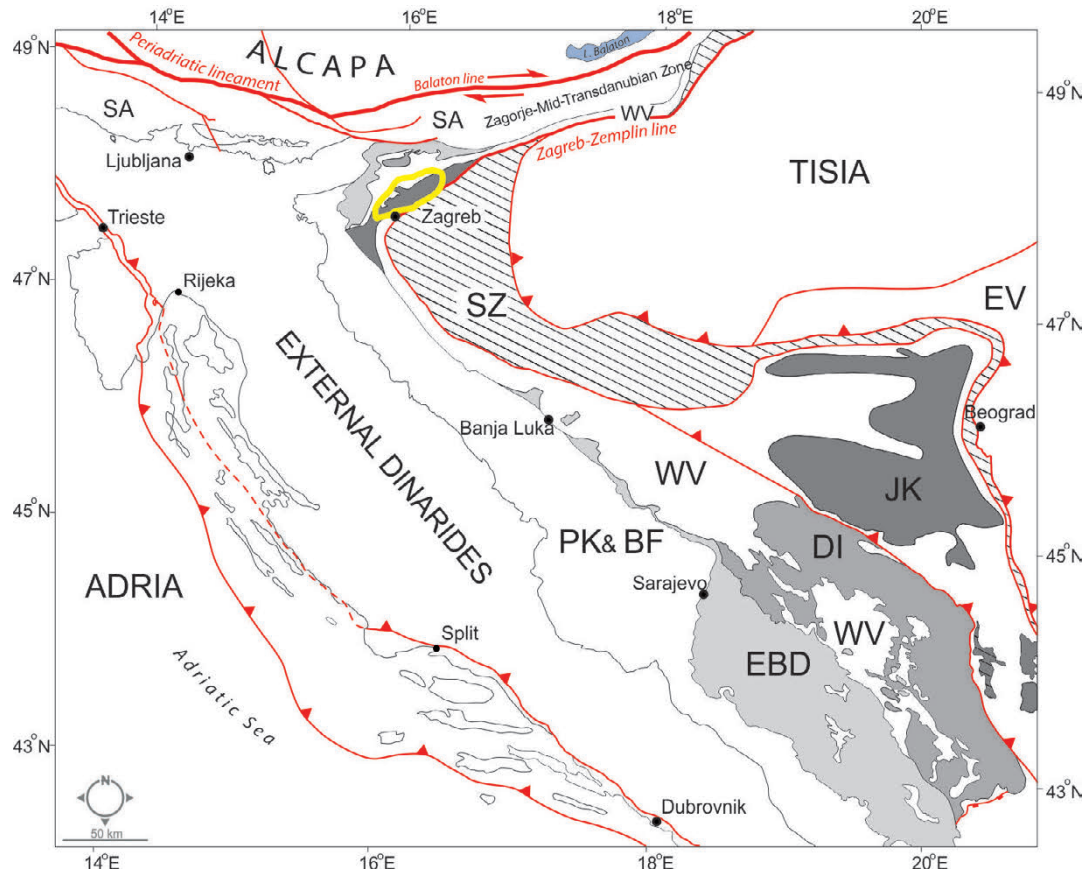


Figure 1. The regional geological position of Medvednica Mountain, compiled after SCHMID et al. (2016). SA – Southern Alps; Ophiolitic units; SZ – Sava zone; WV – Western Vardar units; EV – Eastern Vardar units; Adria derived units: PK&BF – Pre-Karst & Bosnian flysch zone; EBD – East Bosnian - Durmitor; DI – Drina Ivanjica units; JK – Jadar - Kopaonik units. Yellow ellipse marks the position of the Medvednica Mt.

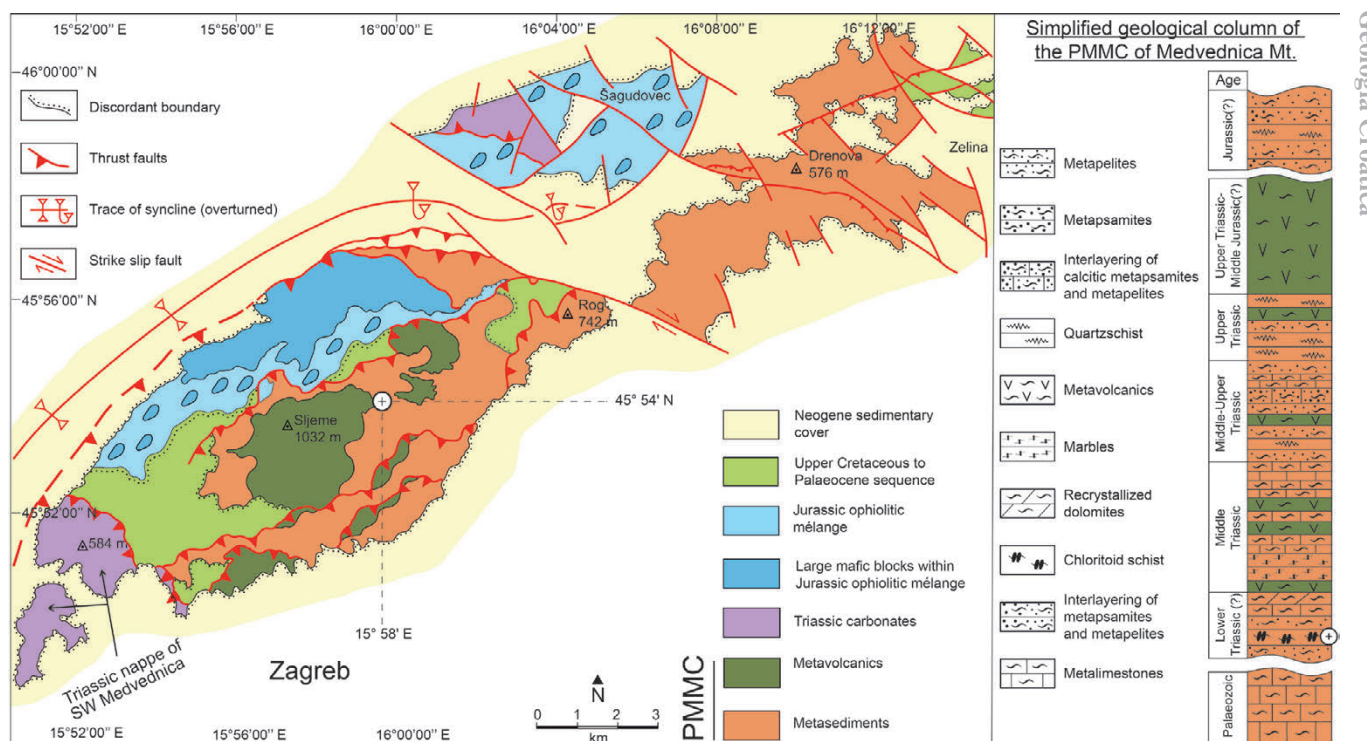


Figure 2. A simplified geological map of Medvednica Mt. (modified after TOMIJEVNOVIĆ et al., 2008). The cross indicates the sampling site. On the right hand side is a simplified schematic geological column of the Palaeozoic-Mesozoic Metamorphic Complex (PMMC) of the Medvednica Mt., the white circle with the cross marks sample location (modified after BELAK et al., 2022).

500 °C and 5 – 6 kbar. These pressure conditions are consistent with medium pressures derived from the b_0 unit cell dimension of potassic white mica (JUDIK et al., 2004). Only on the north-east slopes of Medvednica Mt., blueschist-facies metamorphic rocks occur (BELAK & TIBLJAŠ, 1998).

This study on chloritoid schist from the metasedimentary sequence of the PMMC is based on a sample taken from the southern slope of Medvednica Mt. in the source area of the Stari Potok creek (Fig. 2). The outcrop comprises metapelites to minor metapsammitic rocks and sparse metapelite interlayers. Further up the sequence from this outcrop, the metasedimentary succession is in unconformable contact with tectonized metavolcanics, which are locally intercalated with recrystallized limestone dated by fossils to the Middle Triassic (BELAK, 2005). Based on macroscopic investigations, five samples (ST-1, ST-2, ST-4, ST-5, ST-6) were chosen for petrographic and whole-rock analyses. In addition, a chloritoid schist (sample ST-6) was chosen for monazite dating, thermodynamic modelling and mineral analyses.

3. MATERIALS AND METHODS

3.1. Whole-rock chemistry

The five selected specimens were powdered; air-dried powders were sieved through a 0.125 mm stainless-steel screen. Whole-rock geochemical data were provided by the Bureau Veritas Commodities Canada Ltd. The sample preparation procedure included melting of 0.2 g rock powder mixed with lithium metaborate/tetraborate ($\text{LiBO}_2/\text{Li}_2\text{B}_4\text{O}_7$) and subsequent dissolution in aqua regia. Uncertainties for the analysis of the prepared solution by inductively coupled plasma optical emission spectroscopy (ICP-OES) of the major elements range from 0.01 – 0.002 wt %. The trace-element uncertainties for the analyses by inductively coupled plasma mass spectrometry (ICP-MS) are assumed to be in the range of 8 – 0.05 ppm with an exception for gold (Au) ana-

lysed with an uncertainty of 0.0005 ppm. The rare-earth element (REE) data were normalized to chondrite (BOYNTON, 1984); other trace-element data were normalized to the Upper Continental Crust (TAYLOR & McLENNAN, 1995). Graphical presentation of selected data was undertaken using GCDkit v.4.1. (JANOUŠEK et al., 2006).

3.2. Mineral chemistry

Quantitative analyses of minerals were obtained with a CAMECA SX100 EMP at the Institute for Mineralogy and Crystal Chemistry, University of Stuttgart (Institut für Mineralogie und Kristallchemie, Universität Stuttgart), Germany. Operating conditions were: accelerating voltage of 15 kV, a beam current of 15 nA, and a beam diameter of about three μm with 20 s counting time (both peak and background). Standards for the measurements were natural minerals and pure oxides (albite, corundum, fayalite, periclase, barite, chromium oxide, wollastonite, orthoclase, rutile, rhodonite). Results were corrected using the PAP correction procedure provided by CAMECA (POUCHOU & PICHOIR, 1984; 1991). Analytical uncertainties are reported in MASSONNE (2012). X-ray compositional maps were produced simultaneously for several elements (Fe, Mg, Mn) by area mapping under conditions of 50 nA, 15 kV, 60 ms per step, and step width of 3 μm . The analytical procedure was described in MASSONNE et al. (2012) and LI et al. (2021).

3.3. Monazite dating

Analyses of monazite were conducted with a CAMECA SX100 EMP at the State Geological Institute of Dionýz Štúr, Slovakia using 15 kV accelerating voltage and 180 nA beam current. The counting times at peak position for the following elements were: 300 s for Pb, 35 s for Th, 80 s for U, 40 s for Y, and 20 – 60 s for REEs with longer times for the heavier REEs, 120 s for As, 20 s for Fe and Sr, and 10 s for S, P, Ca, Al, and Si. Calibration was

conducted with natural (apatite, wollastonite) and synthetic materials, glasses, and pure oxides (Al_2O_3 , SiO_2 , (REE) PO_4 , UO_2 , ThO_2) as reported in MASSONNE (2014). The data were processed by the chemical Th–U–total Pb isochron method described in MONTEL et al. (1996) and SUZUKI & KATO (2008). The presented uncertainties refer to 2σ confidence limits. Final calculations and data presentation were accomplished with the aid of “IsoplotR” (VERMEESCH, 2018).

3.4. P-T calculations

3.4.1. CLASSICAL THERMOBAROMETRY

The empirical geothermometer for chlorite–chloritoid pairs (VIDAL et al., 1999), was applied to the chloritoid schist sample (ST-6). This geothermometer is based on the $\text{Mg}-\text{Fe}^{2+}$ exchange between these minerals. The compositional criteria, <1 wt % MnO and <2 wt % ($\text{Cr}_2\text{O}_3 + \text{MnO} + \text{CaO} + \text{Na}_2\text{O} + \text{K}_2\text{O}$) in chlorite and chloritoid pairs, are fulfilled for this sample. Also, the main assumption of equilibrium between chlorite and chloritoid pairs is achieved by measuring these minerals in contact, or close to each other, at the rim of corresponding grains (VIDAL et al., 1999).

Chlorite thermometry is based on the content of tetrahedrally coordinated Al in chlorite. VIDAL et al. (2016) argued that this type of geothermometry results in geologically relevant temperature estimates for chlorite formed at low temperatures (<300 °C) under the assumption that all iron is ferrous. However, at higher formation temperatures, calculated temperatures can scatter (VIDAL et al., 2016). We used the most recent calibration by INOUE et al. (2018).

Phengite barometry, as experimentally calibrated by MASSONNE & SCHREYER (1989) and MASSONNE & SZPURKA (1997), was applied according to CADDICK & THOMPSON (2008). This temperature-dependent barometer is based on incorporating Mg and Fe^{2+} in potassic white mica according to Tschermak's substitution.

3.4.2. PSEUDOSECTIONS – THERMODYNAMIC MODELLING

Isochemical phase diagrams (i.e. pseudosections) were constructed with PERPLE_X (version 6.8.8. downloaded from: <http://www.perplex.ethz.ch/>, CONNOLLY, 1990; 2005; CONNOLLY & PETRINI, 2002). The P-T range of 0.2 to 1.2 GPa and 300 to 600 °C and the system $\text{Mn-Na}_2\text{O-Ca-O-K}_2\text{O-FeO-MgO-Al}_2\text{O}_3-\text{SiO}_2-\text{H}_2\text{O-TiO}_2-\text{O}_2$ were considered. The water content was increased to excess, presuming that water-saturated conditions prevailed at peak P-T conditions.

For the PERPLE_X calculations, the whole-rock composition of ST-6 had to be adjusted: (1) iron and O_2 were corrected for different Fe^{3+} contents, for instance, to fit the assumption that 10% of iron was trivalent during metamorphism (see LO PÒ & BRAGA, 2014), (2) phosphorus was eliminated, but a proportional quantity of calcium was subtracted from the whole-rock analysis as this element is mainly bound in apatite ($\text{Ca}_5(\text{PO}_4)_3\text{OH}$, a correction was not performed for other phosphates as their abundances are minor compared to apatite), and (3) the whole-rock composition including the selected H_2O content was normalized to 100%. The solid-solution models by WHITE et al. (2014) were used: Bi(W) for biotite, Chl(W) for chlorite, Crd(W) for cordierite, Ctd(W) for chloritoid, Gt(W) for garnet, Ilm(WPH) for ilmenite, Mica(W) for white mica, St(W) for staurolite. For feldspars, the model by FUHRMAN & LINDSLEY (1988) was applied. Contouring of the P-T pseudosections by isopleths for the Si content in phengite, Fe content in chlorite and Fe content in chloritoid was also achieved with the PERPLE_X software.

4. RESULTS

4.1. Petrography of the samples

Five samples of metasediments were collected from the lithological succession in the vicinity of the source of the Stari potok (Tab. 1). The only sample with chloritoid (ST-6), occurring at the top of this succession at a small outcrop (Fig. 3A), was chosen for a detailed study of the peak metamorphic conditions. The four other selected samples are quartz schist (ST-1, ST-4) and quartz-sericite-chlorite schist (ST-2, ST-5), for which no mineral analyses were performed (Tab. 1). The minerals in samples ST-2 and ST-5 comprise ca. 60 vol% quartz, ca. 30 vol% white mica (without distinguishing between muscovite, paragonite, margarite and celadonite following PARRY et al., 1984; ARBIOL et al., 2021), ca. 5 vol% chlorite, and ca. 3 vol% plagioclase. The rest is dominated by opaque minerals. Samples ST-1 and ST-4 comprise ca. 80 vol% quartz and ca. 15–20 vol% white mica; the rest is composed mainly of chlorite and opaque minerals.

The S_1 foliation is pronounced in all the investigated schists. Samples ST-2 and ST-5 are lepido-granoblastic, consisting of micro-lithons composed of quartz and plagioclase, and show cleavage domains mainly composed of syn-metamorphic white mica, chlorite, and opaque minerals. Zircon, apatite, tourmaline and rutile were found as accessory phases in all samples.

Chloritoid schist ST-6 is grey in colour and has silky lustre (due to the high content of white mica). Foliation and cleavage are easily discernible, (Fig. 3B). The sample contains chloritoid porphyroblasts visible as dark, short prismatic grains. Major minerals observed in sample ST-6 are quartz (ca. 70 vol%), white mica (ca. 15 vol%), chloritoid (ca. 10 vol%), chlorite (ca. 3 vol%), and opaque minerals (ca. 1–2 vol%). Accessory phases are zircon, baddeleyite (usually as zircon overgrowth), rutile, apatite, tourmaline, monazite, and xenotime. Two distinct mineralogical domains occur which are either mainly composed of white mica or recrystallized quartz-rich micro-lithons. The shape and orientation of white mica flakes and quartz micro-lithons indicate a ‘C-type shear band cleavage microstructure (Fig. 3C) (PASSCHIER & TROUW, 2005). Microstructure S_1 is recognized as a metamorphic structure parallel to C-type shear bands (Fig. 3C) and mica-rich cleavage domains (PASSCHIER & TROUW, 2005). Remnant sedimentary bedding planes (S_0) are not discernible. Chloritoid porphyroblasts are 0.5–2 mm in diameter and show a hypidiomorphic shape (Fig. 3C; D; E). Syntectonic growth is evident in rotated and fractured porphyroblasts (Fig. 3C; D; E). Chloritoid grains are characterized by polysynthetic twins, hourglass-sector zoning, and rare radial aggregates (Fig. 3C; D; E). This zoning is ascribed to fast growth along non-{001} faces resulting in the incorporation of inclusions, while the growth along {001} faces is

Table 1. Locations of samples ST-1, ST-2, ST-4, ST-5, ST-6 and their analysis.

Sample	Northing	Easting	Description	Applied methods
ST-1	5085642	460049	quartz, schist/metapelite	Pet; WR;
ST-2	5085788	459964	quartz, chloritic to sericitic schist/metapelite	Pet; WR;
ST-4	5085808	459724	quartz, schist/metapelite	Pet; WR;
ST-5	5085796	459685	quartz, chloritic to sericitic schist/metapelite	Pet; WR;
ST-6	5085804	459623	quartz, chloritoid, chlorite, sericite schist/metapelite	Pet; WR; EMPA

(Coordinates are presented in HTRS96 reference system, EPSG: 3765) (Pet – petrographical investigation under polarising microscope; WR – whole rock analysis; EMPA – electron microprobe analysis)

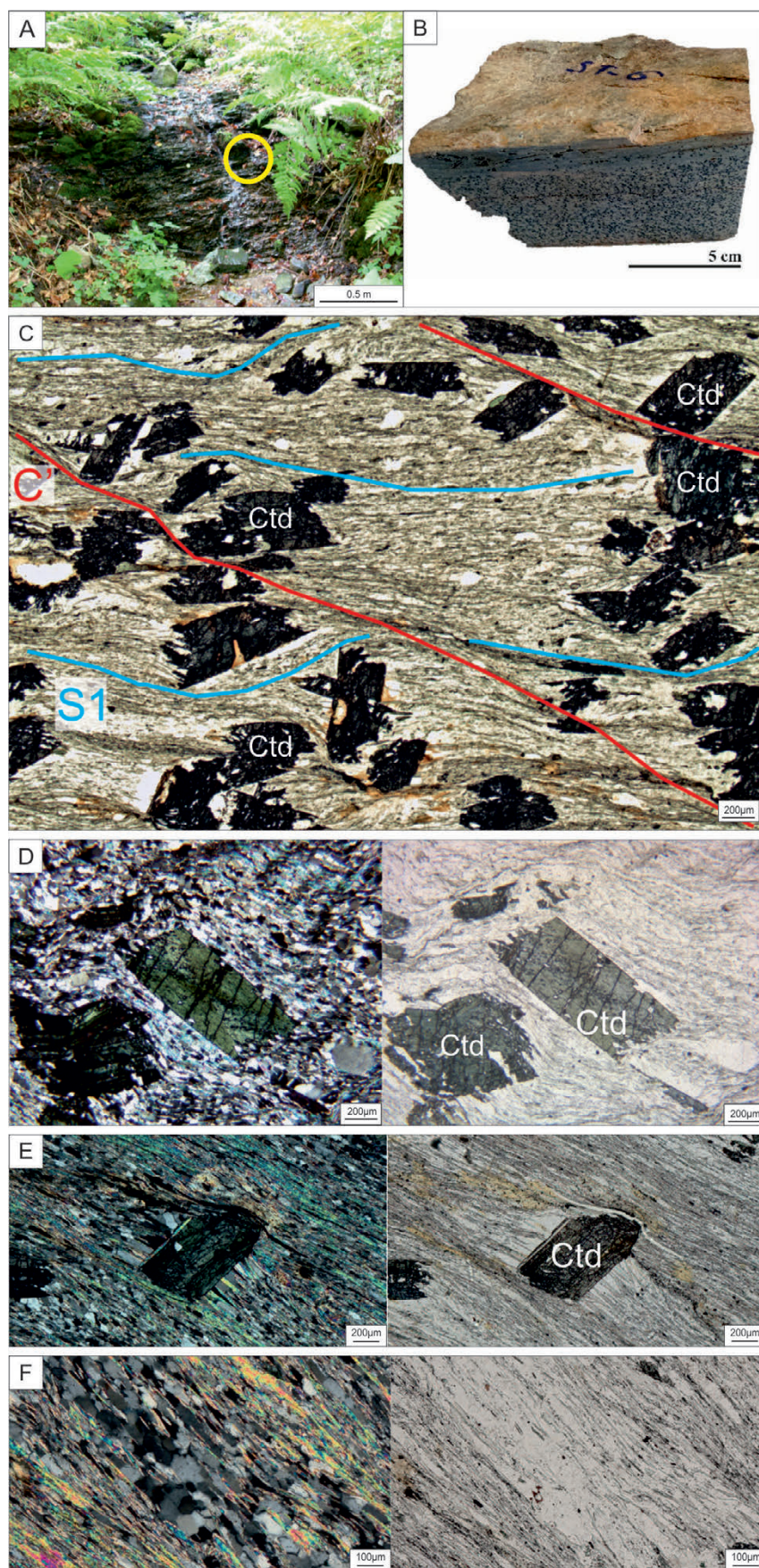


Figure 3. Photographs of chloritoid schist from Medvednica Mt. (sample ST-6). A) Outcrop of the chloritoid schist; the yellow circle marks the sampling location. B) Hand specimen of the chloritoid schist (dark grains are chloritoid crystals). C) Photomicrograph of sample ST-6; cyan lines mark the S1 foliation and red lines C'shear bands. D) Photomicrograph of sample ST-6 (crossed polarizers), fractured chloritoid grain of prismatic habitus with visible hourglass sector zoning; on the right hand side is the same object seen under plane polarized light. E) Photomicrograph of chloritoid with quartz pressure shadows; on the right hand side is the same object seen under plane polarized light. F) Photomicrograph with visible quartz recrystallization boundaries (crossed polarizers); on the right hand side is the same features seen under plane polarized light.

slower ensuring enough time for dissolution and dispersion of excess material (VERNON, 2004; CAMILLERI, 2018). Strain shadows filled with polygonal and elongated quartz are discerned at the boundary of chloritoid grains (Fig. 3D). Quartz grains are equigranular, with sharp polygonal, slightly elongated boundaries, often oriented parallel to S_1 , indicating subgrain rotation recrystallization (SGR) and grain boundary migration recrystallization (GBM, Fig. 3F) (PASSCHIER & TROUW, 2005). Quartz is preferentially bounded by white mica (Fig. 3F). Chlorite grains are mostly elongated with polygonal boundaries and are up to 250 μm in size. Monazite grains are of highly irregular shape (amoeboid, lobate and elongated grain shapes prevail) and small in size (<200 μm). These grains are located in the mica-rich domains.

4.2. Whole-rock chemistry

Results of the whole-rock analyses are presented in Table 2. SiO_2 contents are between 75.0 wt% (ST-1) and 88.3 wt% (ST-2). Total iron ranges from 1.07 wt% Fe_2O_3 (ST-5) to 5.38 wt% Fe_2O_3 (ST-1). The REE patterns of the samples normalized to chondrite (BOYNTON, 1984) are similar in all the studied samples, showing higher values of light REEs compared to heavy REEs ($(\text{La}/\text{Sm})_{\text{N}} = 4.8 - 6.5$) and negative Eu anomalies ($\text{Eu}/\text{Eu}^* = 0.65 - 0.78$) (see Fig. 4). On the diagram of the trace elements normalized to Upper Continental Crust (UCC, TAYLOR & MCLENNAN, 1995), Ba, Ta, Nb and particularly Sr show negative anomalies (Fig. 4). Chloritoid schist ST-6 is characterized by similar values of the major and trace elements as the chloritoid-free samples (Tab. 2; Fig. 4).

4.3. Chemistry of the main minerals in the chloritoid schist

Compositions of chlorite in sample ST-6 are presented in Table 3A. The chlorite formula was calculated on the basis of 14 oxygen atoms. All iron was considered as Fe^{2+} . Due to the small size of the grains, the possible zonation of chlorite remains ambiguous.

Table 2. Bulk rock compositions for samples: ST-1, ST-2, ST-4, ST-5, and ST-6. For comparison samples of chloritoid schists, D7 (MIŠUR et al., 2013) and VrMa (VRAGOVIĆ & MAJER, 1979b) were added.

Sample	ST 1	ST 2	ST 4	ST 5	ST 6	D 7	VrMa
Major elements (wt%)							
SiO ₂	74.98	88.29	75.86	85.65	83.86	74.79	65.75
Al ₂ O ₃	10.96	4.94	10.92	8.38	8.67	13.22	20.43
Fe ₂ O ₃	5.38	2.40	6.59	1.07	3.27	4.73	4.83
MgO	1.55	0.89	0.69	0.42	0.42	0.99	1.79
CaO	0.15	0.24	0.97	0.03	0.06	0.08	
Na ₂ O	1.16	0.82	0.12	0.37	0.08	0.14	0.86
K ₂ O	1.84	0.59	1.04	1.90	1.47	2.50	2.51
TiO ₂	0.72	0.26	0.62	0.48	0.40	0.70	0.90
P ₂ O ₅	0.11	0.18	0.09	0.02	0.05	0.05	0.02
MnO	0.05	0.06	0.13	<0.01	0.04	0.05	0.05
Cr ₂ O ₃	0.02	0.01	0.01	0.00	0.00	0.01	
LOI	3.00	1.30	2.90	1.60	1.60	2.70	3.18
Sum	99.87	99.95	99.94	99.92	99.95	99.96	100.32
Trace elements (ppm)							
Ba	219.00	138.00	188.00	251.00	165.00	300.00	
Be	<1	1.00	2.00	1.00	3.00	1.00	
Co	11.20	11.30	7.40	2.20	2.60	5.10	
Cs	3.20	0.80	1.90	3.20	1.80	4.30	
Ga	11.20	4.60	11.00	6.70	8.30	15.30	
Hf	9.30	3.00	4.60	9.10	4.90	6.20	
Nb	9.20	4.10	8.60	8.40	6.80	12.30	

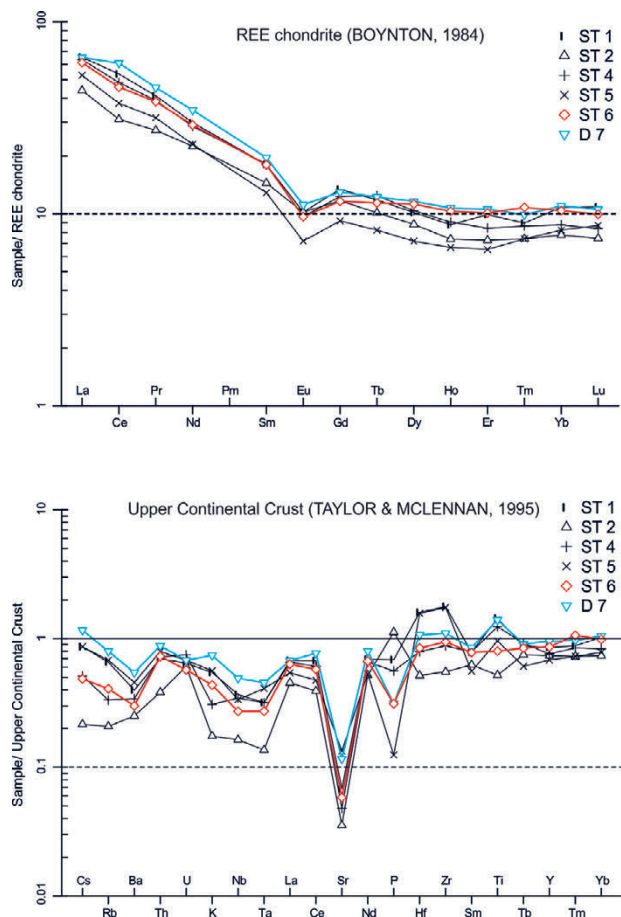


Figure 4. Chondrite normalized REE patterns (REE in chondrite after BOYNTON, 1984) at the top, and Upper Continental Crust normalized spider diagram (trace-elements in Upper Continental Crust, after TAYLOR & MCLENNAN, 1995) at the bottom, for the studied metasediments from Medvednica Mt.. The sample in blue is D7 chloritoid schist from MIŠUR et al. (2013) and the sample in red is the chloritoid schist (ST-6) from this study.

Ni	39.60	27.00	28.00	<20	<20	24.00
Sc	11.00	4.00	9.00	3.00	5.00	12.00
Sr	23.90	12.40	16.80	46.90	20.40	40.70
Ta	0.70	0.30	0.70	0.90	0.60	1.00
Th	7.50	4.10	7.70	8.50	7.80	9.40
U	1.80	1.70	2.10	1.90	1.60	1.90
V	95.00	77.00	78.00	33.00	51.00	95.00
W	1.50	0.90	2.00	1.80	1.50	2.10
Zr	337.40	105.10	167.10	331.60	179.30	208.90
Y	18.80	16.20	16.70	15.00	19.00	21.00
La	20.30	13.60	19.70	16.30	19.00	20.20
Ce	43.20	25.10	39.00	30.40	36.90	49.30
Pr	5.02	3.32	4.75	3.86	4.68	5.54
Nd	17.90	13.50	17.10	13.80	17.40	20.80
Sm	3.52	2.82	3.55	2.51	3.51	3.82
Eu	0.75	0.75	0.71	0.53	0.71	0.82
Gd	3.48	3.03	3.19	2.38	3.01	3.36
Tb	0.56	0.48	0.59	0.39	0.54	0.58
Dy	3.27	2.84	3.34	2.32	3.62	3.74
Ho	0.63	0.53	0.65	0.48	0.74	0.77
Er	2.08	1.53	1.77	1.37	2.12	2.22
Tm	0.29	0.24	0.28	0.24	0.35	0.32
Yb	2.26	1.62	1.83	1.72	2.17	2.30
Lu	0.35	0.24	0.27	0.28	0.32	0.34
Mo	0.30	0.90	<0.1	<0.1	<0.1	<0.1
Cu	47.50	27.90	0.50	0.60	0.30	
Rb	73.40	23.30	37.30	76.10	45.60	89.40
Pb	5.40	8.50	0.70	1.40	4.30	
Zn	92.00	19.00	19.00	8.00	5.00	
Ni	39.60	22.60	17.00	4.20	1.30	24.00
As	4.60	12.80	0.50	1.00	<0.5	
Cd	0.10	<0.1	<0.1	<0.1	<0.1	
Sb	<0.1	<0.1	0.40	<0.1	<0.1	
Bi	<0.1	0.40	0.10	<0.1	<0.1	
Ag	<0.1	<0.1	<0.1	<0.1	<0.1	
Au (ppb)	0.90	<0.5	1.10	<0.5	0.80	
Hg	0.01	<0.01	<0.01	0.02	<0.01	
Tl	<0.1	<0.1	<0.1	<0.1	<0.1	
Se	<0.5	0.60	<0.5	<0.5	<0.5	
SiO ₂ /Al ₂ O ₃	6.84	17.87	6.95	10.22	9.67	
K ₂ O/Na ₂ O	1.59	0.72	8.67	5.14	18.38	
Na ₂ O/K ₂ O	0.63	1.39	0.12	0.19	0.05	
Zr/Hf	36.28	35.03	36.33	36.44	36.59	
Zr/Sc	30.67	26.28	18.57	110.53	35.86	
Zr/Th	44.99	25.63	21.70	39.01	22.99	
Th/Co	0.67	0.36	1.04	3.86	3.00	
Th/Sc	0.68	1.03	0.86	2.83	1.56	
Th/U	4.17	2.41	3.67	4.47	4.88	
Co/Th	1.49	2.76	0.96	0.26	0.33	
Hf/Sc	0.85	0.75	0.51	3.03	0.98	
La/Co	1.81	1.20	2.66	7.41	7.31	
La/Y	1.08	0.84	1.18	1.09	1.00	
La/Yb	8.98	8.40	10.77	9.48	8.76	
La/Sc	1.85	3.40	2.19	5.43	3.80	
La/Sm	5.77	4.82	5.55	6.49	5.41	
La/Th	2.71	3.32	2.56	1.92	2.44	
Y/Ni	0.47	0.72	0.98	3.57	14.62	
(La/Yb) _N	8.98	8.40	10.77	9.48	8.76	
(La/Sm) _N	5.77	4.82	5.55	6.49	5.41	
(Gd/Yb) _N	1.54	1.87	1.74	1.38	1.39	
Eu/Eu*	0.66	0.78	0.65	0.66	0.67	
ΣREE	103.61	69.60	96.73	76.58	95.07	

Table 3A. Selected microprobe analyses of chlorite in the investigated chloritoid schist from Medvednica Mt.

Chlorite		Wt%														A/R														
	1-15	1-18	1-19	1-23	1-25	1-27	1-30	1-46	1-53	2-12	2-49	2-6	2-41	2-9	2-38	2-14	2-3	2-43	2-19	2-1	2-25	2-16	2-45	MIN	MAX					
SiO ₂	24.05	24.31	23.92	23.89	24.00	23.94	23.72	24.70	23.66	23.83	23.63	23.66	23.68	23.68	23.79	23.91	23.93	23.96	23.97	24.11	24.12	25.18	25.31	23.63	25.31	24.03				
TiO ₂	0.02	0.03	0.04	0.05	0.04	0.01	0.02	0.02	0.05	0.06	0.04	0.04	0.02	0.05	0.03	0.03	0.06	0.01	0.03	0.02	0.04	0.02	0.05	0.03	0.01	0.06	0.03			
Al ₂ O ₃	23.14	22.26	23.29	23.04	23.25	23.23	23.29	22.82	23.43	23.07	23.35	23.19	23.15	23.01	23.81	23.43	23.44	23.70	23.33	23.52	23.63	24.27	23.99	24.61	22.26	24.61	23.39			
Cr ₂ O ₃	0.00	0.00	0.00	0.00	0.00	0.00	0.00	0.00	0.00	0.00	0.04	0.05	0.01	0.01	0.03	0.01	0.06	0.04	0.02	0.04	0.01	0.00	0.03	0.02	0.07	0.00	0.07	0.02		
FeO	27.36	26.51	28.57	28.56	27.61	27.28	27.20	28.89	29.08	27.27	27.59	26.97	25.89	27.47	27.73	27.18	27.11	25.85	27.70	26.99	26.68	26.14	25.81	25.81	29.08	27.29				
MnO	0.14	0.11	0.17	0.16	0.17	0.17	0.21	0.15	0.14	0.12	0.16	0.15	0.18	0.17	0.12	0.11	0.09	0.13	0.17	0.12	0.22	0.11	0.14	0.13	0.09	0.22	0.15			
MgO	13.36	14.03	12.72	11.87	13.19	12.72	12.86	12.58	12.06	11.96	12.96	13.07	13.14	13.91	12.85	12.30	12.46	12.83	13.66	12.35	13.47	11.85	12.26	11.27	11.27	14.03	12.74			
Total	88.08	87.26	88.70	87.57	88.26	87.68	87.38	87.48	88.20	88.11	87.47	87.75	87.17	86.68	88.01	87.45	87.18	87.73	87.04	87.68	88.46	87.08	87.80	87.23						
Si	2.55	2.59	2.54	2.57	2.54	2.56	2.54	2.63	2.55	2.53	2.53	2.54	2.54	2.54	2.52	2.55	2.56	2.54	2.55	2.54	2.56	2.54	2.57	2.65	2.67	2.52	2.67	2.56		
Al _{tot}	2.89	2.80	2.91	2.92	2.90	2.92	2.94	2.87	2.95	2.91	2.94	2.92	2.92	2.91	2.98	2.96	2.96	2.97	2.97	2.93	2.96	2.93	3.05	2.97	3.06	2.80	3.06	2.94		
v/Al	1.45	1.41	1.46	1.43	1.46	1.44	1.46	1.37	1.47	1.45	1.47	1.47	1.46	1.46	1.48	1.45	1.44	1.46	1.46	1.45	1.44	1.46	1.44	1.43	1.35	1.33	1.48	1.44		
Ti	0.00	0.00	0.00	0.00	0.00	0.00	0.00	0.00	0.00	0.00	0.00	0.00	0.00	0.00	0.00	0.00	0.00	0.00	0.00	0.00	0.00	0.00	0.00	0.00	0.00	0.00	0.00			
Fe ²⁺	2.43	2.37	2.53	2.57	2.45	2.46	2.44	2.42	2.58	2.60	2.44	2.46	2.42	2.32	2.44	2.48	2.43	2.41	2.30	2.47	2.38	2.38	2.30	2.28	2.28	2.60	2.43			
Mn	0.01	0.01	0.01	0.01	0.02	0.02	0.01	0.01	0.01	0.01	0.01	0.01	0.01	0.01	0.01	0.01	0.01	0.02	0.01	0.01	0.01	0.01	0.01	0.01	0.02	0.01	0.01			
Mg	2.11	2.23	2.01	1.90	2.08	2.02	2.05	2.00	1.92	1.91	2.07	2.08	2.10	2.22	2.03	1.96	1.99	2.03	2.17	1.96	2.11	1.88	1.92	1.77	1.77	2.23	2.02			
$\Sigma_{\text{Oct}} \text{ (Fe,Mg,Al)}$	5.99	5.99	5.99	5.95	5.98	5.97	5.97	5.92	5.98	5.97	5.99	5.98	5.97	5.99	5.97	5.94	5.96	5.95	5.97	5.95	5.97	5.89	5.84	5.78	5.78	5.99	5.95			
Σ_{VacOct}	0.01	0.01	0.05	0.02	0.03	0.03	0.08	0.02	0.03	0.01	0.02	0.01	0.03	0.05	0.06	0.04	0.05	0.03	0.11	0.16	0.22	0.01	0.22	0.05						
XFe=																														
Fe/(Fe+Mg+Mn)	0.53	0.51	0.56	0.57	0.54	0.55	0.54	0.55	0.57	0.58	0.54	0.54	0.51	0.55	0.56	0.55	0.54	0.52	0.56	0.53	0.56	0.54	0.56	0.51	0.58	0.55				
XMg	0.47	0.49	0.44	0.43	0.46	0.45	0.46	0.43	0.42	0.46	0.46	0.46	0.46	0.46	0.46	0.45	0.45	0.45	0.46	0.46	0.47	0.44	0.46	0.44	0.42	0.49	0.45			

Chlorite formulae calculated on basis of 14 oxygen atoms and iron was considered as Fe²⁺. * $\Sigma_{\text{Oct}} \text{ (Fe,Mg,Al)}$ is the sum of cations in the octahedral position, ** Σ_{VacOct} represents vacancies at the octahedral positions.

Table 3B. Selected microprobe analyses of muscovite in the investigated chloritoid schist from Medvednica Mt.

Muscovite

Wt%	1-11	1-12	1-16	1-17	1-20	1-28	1-29	1-50	1-52	MIN	MAX	AVR
SiO ₂	46.73	46.17	45.54	45.94	45.61	45.89	45.37	46.07	45.91	45.37	46.73	45.91
TiO ₂	0.25	0.13	0.12	0.06	0.15	0.15	0.07	0.12	0.11	0.06	0.25	0.13
Al ₂ O ₃	34.79	34.76	34.89	35.30	34.72	34.98	35.12	35.15	35.44	34.72	35.44	35.02
FeO	2.32	2.26	3.05	2.72	2.67	2.22	2.54	2.33	2.92	2.22	3.05	2.56
MnO	0.00	0.00	0.03	0.01	0.01	0.00	0.00	0.00	0.01	0.00	0.03	0.01
MgO	0.47	0.59	0.45	0.46	0.49	0.54	0.40	0.55	0.44	0.40	0.59	0.49
CaO	0.03	0.00	0.00	0.00	0.01	0.00	0.00	0.02	0.00	0.00	0.03	0.01
Na ₂ O	0.62	0.61	0.55	0.64	0.58	0.57	0.64	0.56	0.54	0.54	0.64	0.59
K ₂ O	10.44	10.26	10.61	10.01	10.29	10.69	10.61	10.39	10.45	10.01	10.69	10.42
BaO	0.13	0.05	0.18	0.15	0.21	0.14	0.15	0.12	0.11	0.05	0.21	0.14
H ₂ O	4.51	4.48	4.46	4.49	4.45	4.47	4.44	4.49	4.50	4.44	4.51	4.48
Total	100.29	99.30	99.89	99.78	99.18	99.66	99.34	99.80	100.44			

Si	3.11	3.10	3.06	3.07	3.08	3.08	3.06	3.08	3.06	3.06	3.11	3.08
Ti	0.01	0.01	0.01	0.00	0.01	0.01	0.00	0.01	0.01	0.00	0.01	0.01
Al _{TOT}	2.73	2.75	2.77	2.78	2.76	2.77	2.79	2.77	2.79	2.73	2.79	2.77
Al ^{IV}	0.89	0.90	0.94	0.93	0.92	0.92	0.94	0.92	0.94	0.89	0.94	0.92
Al ^{VI}	1.84	1.85	1.83	1.86	1.84	1.85	1.85	1.85	1.85	1.83	1.86	1.84
Fe ⁺²	0.13	0.13	0.17	0.15	0.15	0.12	0.14	0.13	0.16	0.12	0.17	0.14
Mn	0.00	0.00	0.00	0.00	0.00	0.00	0.00	0.00	0.00	0.00	0.00	0.00
Mg	0.05	0.06	0.05	0.05	0.05	0.05	0.04	0.05	0.04	0.04	0.06	0.05
Ca	0.00	0.00	0.00	0.00	0.00	0.00	0.00	0.00	0.00	0.00	0.00	0.00
Na	0.08	0.08	0.07	0.08	0.08	0.07	0.08	0.07	0.07	0.07	0.08	0.08
K	0.89	0.88	0.91	0.85	0.89	0.92	0.91	0.89	0.89	0.85	0.92	0.89
Ba	0.00	0.00	0.00	0.00	0.00	0.00	0.00	0.00	0.00	0.00	0.00	0.00
H	2.00	2.00	2.00	2.00	2.00	2.00	2.00	2.00	2.00	2.00	2.00	2.00
Total	9.72	9.75	9.80	9.78	9.77	9.79	9.83	9.78	9.80			

Muscovite formulae calculated on basis of 11 oxygen atoms and all iron was considered as Fe²⁺

The composition of chlorite is characterized by FeO and MgO contents between 25.8 and 29.1 wt% and 11.3 and 14 wt%, respectively (24 measurements, Tab. 3A). The average composition of chlorite shows 1.44 atoms per formula unit (apfu) of tetrahedrally coordinated Al. Average XFe = Fe²⁺/(Mg+Fe²⁺+Mn) is 0.55. The abundances of Ti and Mn are almost negligible (Tab. 3A). The chemical compositions of chlorite show a uniform pattern and correspond to the ripidolite-chamosite series on the octahedral Fe/(Fe+Mg) versus tetrahedral Al diagram after FOSTER (1962) and BAILEY (1980) as shown in Figure 5A. According to the ternary Mg – (Al+Vac^{oct}) – Fe²⁺ diagram after ZANE & WEISS (1998), chlorite is a trioctahedral (Type I) Fe-chlorite (Fig. 5B). The ternary (Fe+Mg) – Si – Al_{TOT} diagram after ABD ELMOLA et al. (2017) confines the analysed chlorites between daphnite and amesite (Fig. 5C).

Nine EMP analyses were performed on white mica. Only grains of metamorphic origin, characterized by polygonal, elongated and hypidiomorphic habitus, were analysed. The possible zonation of grains remains unclear because of the minute size of the micas. All analyses are given in Table 3B. The structural for-

mula is based on 11 oxygen, resulting in Si values between 3.06 and 3.11 apfu, Na = 0.07 – 0.08 apfu, Fe²⁺ = 0.12 – 0.17 apfu, and interlayer occupancies of 0.93 – 0.99 apfu (Tab. 3B). These values classify the white mica in sample ST-6 as muscovite (after ARBIOL et al. 2021 and references therein). On the Al vs. Fe+Mg+Si (apfu) binary diagram, analysed micas follow Tschermak's substitution (Fig. 6B). By the classification principles described in TISCHENDORF et al. (2007) the analysed micas are common true K micas. According to the occupancy of the octahedral layer, the analysed micas belong to the celadonite – muscovite series (Fig. 6C) following the mgli-feal plot (mgli = Mg – Li; feal = (^{VI}Fe_{TOT} + Mn + Ti) - ^{VI}Al, after; ARBIOL et al., 2021; TISCHENDORF et al., 2007). Also, the Fe/Al₂O₃ versus Mg/Al₂O₃ ratios of the analysed micas uniformly plot in the muscovite field (Fig. 6D) (see ARBIOL et al., 2021).

Forty-nine EMP analyses were performed on chloritoid grains. Chemical mapping was performed on two selected chloritoid blasts and showed slight Mg enrichment and Mn depletion from the core towards the rim (Fig. 7A; B). All grains show similar chemical compositions (Tab. 3C). Chloritoid is characterized

Table 3C. Selected microprobe analyses of chloritoid in the investigated chloritoid schist from Medvednica Mt.

		Chloritoid																								
		rim					core					core					rim									
Wt%		1-1	1-4	1-5	1-6	1-7	1-8	1-9	1-10	1-14	1-21	1-32	1-33	1-34	1-35	1-36	1-37	1-38	1-39	1-40	1-41	1-49	1-51	1-53	2-42	2-50
SiO ₂	24.10	24.17	23.93	23.96	23.80	23.99	24.13	24.13	23.99	23.43	23.76	23.80	23.99	23.94	23.80	24.03	23.89	24.00	23.98	24.09	23.96	24.00	23.82	24.13	22.89	23.01
TiO ₂	0.02	0.02	0.00	0.02	0.00	0.01	0.04	0.17	0.05	0.00	0.00	0.00	0.00	0.03	0.00	0.02	0.01	0.01	0.01	0.01	0.03	0.00	0.55	0.02	0.00	0.00
Al ₂ O ₃	39.35	39.60	39.63	39.78	39.09	39.96	39.80	39.82	39.80	39.43	39.08	39.26	39.54	39.17	39.23	39.12	39.43	39.27	39.48	39.26	39.54	39.30	39.40	40.08	39.55	39.43
FeO	26.14	26.41	25.78	25.53	26.55	25.94	25.85	26.22	25.60	24.94	26.59	25.85	26.02	26.20	26.40	26.10	25.80	25.62	25.68	25.97	25.79	25.70	25.08	25.32	25.06	25.70
MnO	0.00	0.34	0.41	0.41	0.38	0.41	0.28	0.30	0.44	0.40	0.35	0.44	0.43	0.38	0.45	0.42	0.35	0.39	0.33	0.33	0.37	0.34	0.36	0.32		
MgO	2.69	2.75	2.77	2.93	2.71	2.71	2.99	2.67	2.75	2.90	2.66	2.76	2.85	2.63	2.66	2.66	2.78	2.75	2.75	2.79	2.60	2.85	2.67	2.69	2.77	
Total	92.30	93.29	92.53	92.62	92.55	92.98	93.19	93.15	92.61	91.18	92.48	92.02	92.76	92.40	92.51	92.19	92.24	92.10	92.25	92.46	92.43	91.92	92.06	92.55	90.54	91.24
ap.f.u.																										
Si	2.00	1.99	1.98	1.98	1.97	1.98	1.98	1.98	1.96	1.97	1.98	1.98	1.99	1.97	2.00	1.98	1.99	1.99	1.99	2.00	1.98	2.00	1.99	1.93	1.93	
Ti	0.00	0.00	0.00	0.00	0.00	0.00	0.00	0.00	0.01	0.00	0.00	0.00	0.00	0.00	0.00	0.00	0.00	0.00	0.00	0.00	0.00	0.03	0.00	0.00	0.00	
Al	3.85	3.84	3.87	3.87	3.82	3.88	3.85	3.86	3.88	3.89	3.82	3.88	3.85	3.85	3.83	3.84	3.84	3.86	3.85	3.86	3.84	3.86	3.86	3.90	3.94	3.90
Fe ²⁺	1.67	1.65	1.65	1.63	1.66	1.67	1.63	1.66	1.64	1.67	1.65	1.64	1.64	1.66	1.67	1.66	1.65	1.63	1.64	1.64	1.65	1.64	1.65	1.70	1.70	
Fe ³⁺	0.15	0.16	0.13	0.13	0.18	0.12	0.15	0.14	0.11	0.10	0.18	0.15	0.15	0.16	0.16	0.16	0.16	0.15	0.14	0.16	0.14	0.14	0.11	0.10	0.06	0.10
Mn	0.00	0.02	0.03	0.03	0.03	0.03	0.02	0.02	0.03	0.03	0.02	0.02	0.03	0.03	0.03	0.03	0.03	0.03	0.03	0.02	0.02	0.03	0.02	0.03	0.02	
Mg	0.33	0.34	0.34	0.36	0.34	0.33	0.37	0.33	0.34	0.36	0.33	0.34	0.35	0.34	0.33	0.33	0.32	0.33	0.34	0.34	0.34	0.32	0.35	0.33	0.34	0.35
Total	8.00	8.00	8.00	8.00	8.00	8.00	8.00	8.00	8.00	8.00	8.00	8.00	8.00	8.00	8.00	8.00	8.00	8.00	8.00	8.00	8.00	8.00	8.00	8.00	8.00	
XFe=																										
Fe/(Fe+Mg+Mn)	0.85	0.83	0.83	0.82	0.83	0.83	0.82	0.84	0.83	0.83	0.82	0.84	0.83	0.84	0.84	0.84	0.83	0.83	0.83	0.84	0.82	0.83	0.83	0.83	0.83	

Chloritoid formulae calculated on basis of 12 oxygen atoms, iron was calculated as Fe³⁺=4(Al+Ti)

Table 3C (continued).

	rim		core		rim		core		core		rim		rim		rim	
	rim	rim	rim	core	rim	core	rim	core	rim	core	rim	rim	rim	rim	rim	rim
W%	2.35	2.34	2.26	2.28	2.48	2.44	2.33	2.20	2.24	2.39	2.29	2.31	2.22	2.32	2.46	2.15
SiO ₂	23.06	23.07	23.11	23.12	23.18	23.19	23.30	23.30	23.39	23.41	23.46	23.52	23.54	23.64	23.72	23.73
TiO ₂	0.02	0.84	0.01	0.00	0.01	0.05	0.00	0.00	0.02	0.00	0.02	0.02	0.02	0.05	0.00	0.00
Al ₂ O ₃	39.83	38.92	38.99	38.88	39.74	39.58	39.63	39.59	39.13	39.38	40.41	38.91	39.16	39.51	39.69	39.72
FeO	25.56	25.60	26.05	25.20	24.36	24.77	25.64	25.26	25.84	25.23	24.70	25.94	26.06	25.13	25.20	25.06
MnO	0.36	0.35	0.35	0.38	0.38	0.35	0.45	0.38	0.34	0.35	0.41	0.35	0.52	0.37	0.51	0.46
MgO	2.66	2.76	2.64	2.70	3.05	2.85	2.75	2.93	2.76	2.73	2.82	2.67	2.79	2.92	2.64	2.67
Total	91.48	91.53	91.15	90.28	90.72	90.75	91.78	91.52	91.45	91.11	91.83	91.40	92.10	91.58	91.78	91.66
ap.f.u.																
Si	1.93	1.94	1.94	1.96	1.95	1.95	1.94	1.95	1.96	1.97	1.95	1.97	1.96	1.97	1.98	1.97
Ti	0.00	0.05	0.00	0.00	0.00	0.00	0.00	0.00	0.00	0.00	0.00	0.00	0.00	0.00	0.00	0.00
Al	3.93	3.85	3.87	3.89	3.93	3.92	3.90	3.90	3.86	3.90	3.96	3.85	3.84	3.88	3.90	3.91
Fe ⁺²	1.71	1.70	1.70	1.67	1.64	1.67	1.68	1.66	1.67	1.67	1.66	1.64	1.66	1.67	1.66	1.65
Fe ⁺³	0.07	0.10	0.13	0.11	0.07	0.08	0.10	0.10	0.14	0.10	0.04	0.15	0.16	0.12	0.10	0.09
Mn	0.03	0.02	0.03	0.03	0.03	0.03	0.03	0.03	0.02	0.03	0.04	0.03	0.04	0.03	0.02	0.02
Mg	0.33	0.34	0.33	0.34	0.38	0.36	0.34	0.36	0.34	0.35	0.33	0.35	0.36	0.33	0.33	0.34
Total	8.00	8.00	8.00	8.00	8.00	8.00	8.00	8.00	8.00	8.00	8.00	8.00	8.00	8.00	8.00	8.00
XFe= Fe/(Fe+Mg+Mn)	0.83	0.83	0.84	0.83	0.81	0.82	0.83	0.82	0.83	0.83	0.82	0.84	0.83	0.83	0.82	0.83

Chloritoid formulae calculated on basis of 12 oxygen atoms, iron was calculated as $\text{Fe}^{3+}=4(\text{Al}+\text{Ti})$

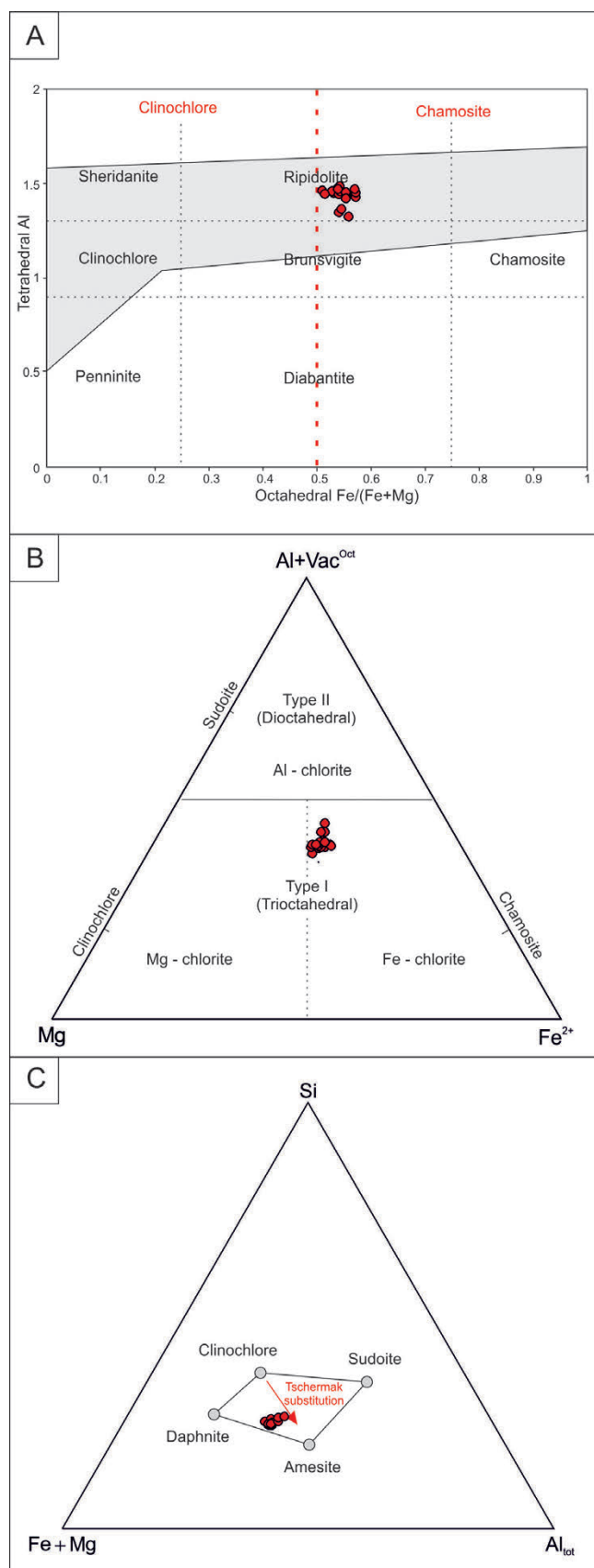


Figure 5. Chlorite classification diagrams for chloritoid schist, sample ST-6 (in red circles), from Medvednica Mt. A) Octahedral $\text{Fe}/(\text{Fe} + \text{Mg})$ versus tetrahedral Al diagram with different classes of Fe-Mg chlorite (classification after FOSTER, 1962; clinochlore-chamosite boundary (vertical dashed line) after BAILEY, 1980; chlorite polytype area in grey colour after FOSTER, 1962). B) Compositional field of chlorite (after ZANE & WEISS, 1998). Type I chlorite is dominantly Mg-Fe chlorite, depending on the dominant cation. Type II chlorite is dominantly Al-chlorite. C) $\text{Fe} + \text{Mg} - \text{Si} - \text{Al}(\text{total})$ ternary diagram (after ABD ELMOLA et al., 2017).

by $\text{Fe}^{3+} = 0.04 - 0.18 \text{ apfu}$, $\text{Fe}^{2+} = 1.62 - 1.71 \text{ apfu}$, $\text{Mn} = 0.00 - 0.04 \text{ apfu}$, and $\text{Mg} = 0.32 - 0.38 \text{ apfu}$ based on calculations with 12 oxygen and 8 cations (without H_2O).

4.4. Chemistry and age of monazite

The EMP chemical dating data on monazite are presented in Table 4 and Figure 8. The structural calculations are based on 16 oxygen atoms. The examined monazites are characterized by the irregular grain shapes of lobate, amoeboid and elongated contours (Fig. 8A; B). Results of 30 analyses show a range of values for Ce_2O_3 (34.1 – 22.7 wt%), La_2O_3 (15.3 – 4.6 wt%) and Y_2O_3 (0.3 – 1.6 wt%). The ThO_2 contents vary from 1.56 to 5.89 wt%. Low SiO_2 (0.17 – 0.82 wt%) contents and slightly elevated CaO (0.45 – 1.1 wt%) contents characterize the analysed monazite (Tab. 4).

Concentrations of Th, U, and total Pb in 30 analyses were used for chemical age calculations, including uncertainties, utilizing the method as described in MONTEL et al. (1996) and SUZUKI & KATO (2008) (Fig. 9A). Monazite (mnz) analyses are marked using the first symbol to indicate the grain and the second one (after the slash) the number of the analysis. Four analyses (mnz 2/1: 219 ± 19 Ma; mnz C/1: 211 ± 18 Ma; mnz 3/1x: 192.50 ± 16.70 Ma and mnz I/1: 93 ± 8 Ma) were rejected from the weighted mean as outliers by the generalized Chauvenet criterion (CHAUVENET, 1863; empty boxes on Fig. 9A). Based on the crystal chemical composition (see below) the calculated ages from the remaining 26 measurements are separated into two age groups. The calculated weighted mean of 13 measurements of the younger monazite group is 142.95 ± 1.72 Ma with an MSWD value of 1.27. The calculated weighted mean age for the 13 measurements yielding older ages is 167.54 ± 2.01 with an MSWD of 0.45 (Tab. 4, Fig. 9A). The two corresponding ages (143.0 and 167.5 Ma) are visible as plateaus on the weighted mean diagram in Figure 9A. The clustering of ages is compatible with the zonation that was observed in monazite grains on SEM-BSE images (Fig. 8B). Monazite grain mnz 6 with 7 analyses shows an age distribution split into two groups: (1) younger mnz 6/1x, mnz 6/2, mnz 6/3 and mnz 6/7 rim analyses with an average of 143 ± 6.2 Ma and MSWD of 0.38 and (2) older mnz 6/5, mnz 6/4 and mnz 6/1 core analyses with an average of 170 ± 8.5 Ma, MSWD of 0.024 (Fig. 8B). The concentrations of heavy REEs (HREEs) in monazite of the younger age cluster ($n=13$) are lower than in the older monazite ($n=13$) as shown in Figure 9B. In the triangular plot of LREE_2O_3 , $(\text{HREE}_2\text{O}_3 + \text{Y}_2\text{O}_3)_{10}$ and $(\text{ThO}_2 + \text{UO}_2)_{20}$, the younger and older monazite age data can be discriminated (Fig. 9C, after ANDERSSON et al., 2018; PYLE et al., 2001). In the diagram $4(\text{Th} + \text{U} + \text{Pb})$ vs. $4(\text{REE} + \text{Y} + \text{P})$, the measured monazites follow the cheralite substitution ($\text{Ca}(\text{Th}, \text{U})\text{REE}_{-2}$) rather than the huttonite ($(\text{Th}, \text{U})\text{SiREE}_{-1}\text{P}_{-1}$) exchange vector (PYLE et al., 2001; ONDREJKA et al., 2012)(Fig. 9D) with subordinate amounts of cheralite (4 – 9 wt.%) and huttonite (up to 2 wt.%) calculated according to PYLE et al. (2001), (Tab. 4).

4.5. Chloritoid-schist geothermobarometry

To correctly apply the geothermobarometers outlined in section 3.4.1., spots were chosen for the chemical analyses of chlorite, chloritoid and muscovite based on microtextural evaluation of mineral equilibrium using BSE images (Fig. 10). For classical thermometry 10 chlorite - chloritoid pairs were analysed. These pairs were selected based on the criterion given by VIDAL et al. (1999), the main criterion being the achievement and preservation of textural and chemical equilibrium of chloritoid and chlo-

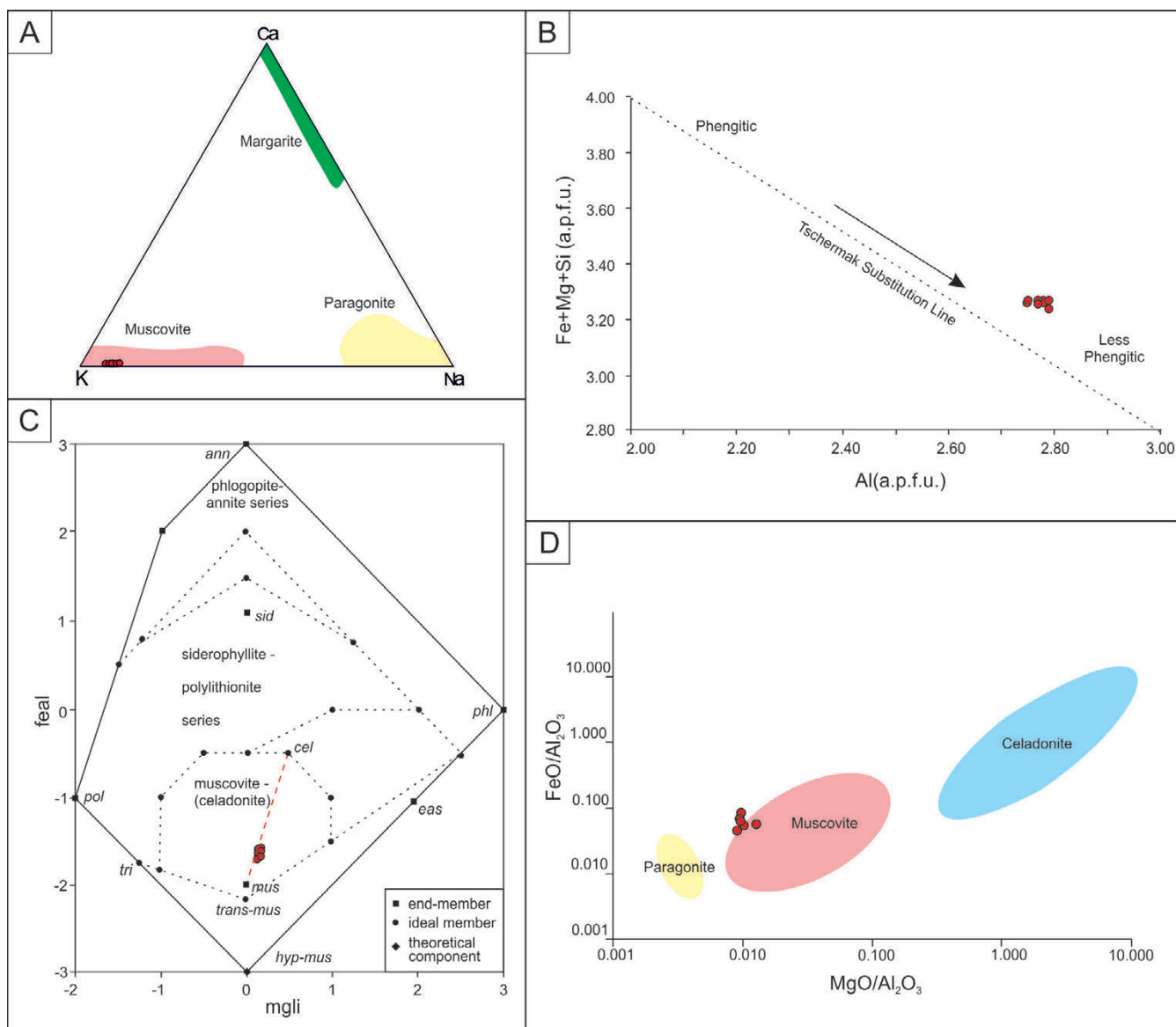


Figure 6. White mica classification diagrams for chloritoid schist from Medvednica Mt., sample ST-6 (in red circles). A) Interlayer K – Na – Ca triangular plot (ARBIOL et al., 2021). B) Al vs. Fe + Mg + Si (apfu) binary diagram with scales of Tschermark substitution of the mica. C) mgli/feal diagram with mica end-members, ideal end-members, and a theoretical component. Prefixes characterize varieties of the muscovite-celadonite series (mgli = Mg – Li; feal = $(^VI\text{Fe}_{\text{tot}} + \text{Mn} + \text{Ti}) - ^VI\text{Al}$, after; ARBIOL et al., 2021; TISCHENDORF et al., 2007). (D) FeO/Al₂O₃ vs. MgO/Al₂O₃ binary diagram (after ARBIOL et al., 2021, and reference therein).

rite grains. With that in mind, nearest neighbours were selected and measured close to the rim (Fig. 10). The temperatures obtained with the Fe²⁺-Mg exchange geothermometer, range between 527 and 568 °C (Fig. 10, Tab. 5).

The application of the chlorite thermometry after INOUE et al. (2018) yielded temperatures between 250 and 598 °C, calculated for 14 selected chlorite grains, which were not in contact with chloritoid grains. This temperature range might indicate that some analysed chlorites did not equilibrate with chloritoid (Fig. 10, Tab. 5).

The nine white mica compositions were used to estimate pressure, resulting in 0.87 to 0.99 GPa at a temperature of 550 °C using the CADDICK & THOMPSON (2008) formulation. This temperature resulted from the previously applied geothermometers. A change of the input temperature by ± 50 °C leads to a pressure change of about ± 0.08 GPa (see Tab. 5).

The P-T pseudosection modelling in the MnNCKFMASHTO system with 0, 5, 10, 15, and 20 % Fe as Fe₂O₃ at water saturation with PERPLE_X led to different P-T conditions by using the rel-

evant mineral compositions (section 4.3.) of chloritoid (XFe = 0.81 – 0.85), chlorite (XFe = 0.51 – 0.58) and muscovite (3.06 – 3.11 Si apfu) (Supplementary 1). For example, at 550 °C (Tab. 5), the Si content (3.07 apfu) in muscovite points to 0.9 GPa in the calculation with 0 % Fe as Fe₂O₃ but to 1.05 GPa with 20 % Fe as Fe₂O₃.

5. DISCUSSION

5.1. Protolith

Considering the field relationships, the petrographical analyses and geochemical analyses, the investigated samples are metamorphosed sediments, originally siltstones and sandstones. Diagenesis and low-grade metamorphism can affect the chemical composition of the source sediments, but the REEs, Th, Sc, and other semimobile to immobile trace elements are usually not affected by these processes and are, thus, useful for comprehending the source rocks (BHATIA & CROOK, 1986; MCLENNAN & TAYLOR, 1991; CULLERS, 2002; BALEN et al., 2013). High values

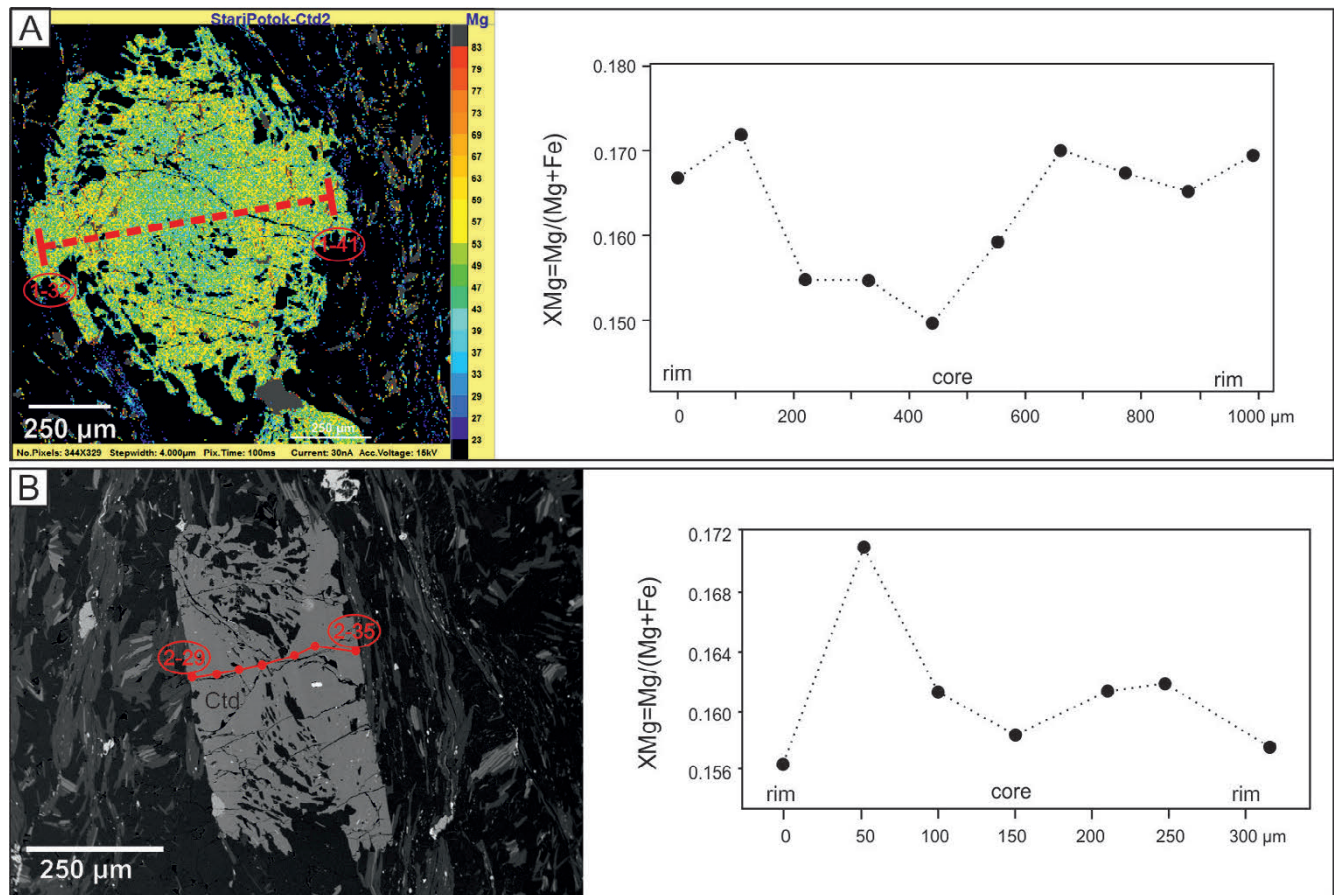


Figure 7. Chemical maps of two analysed chloritoids from Medvednica Mt. (sample ST-6). A) X_{Mg} distribution map obtained from a chloritoid grain with the EMP. The measuring pattern is marked in red. On the right is the associated diagram of the measured profile with X_{Mg} values across the chloritoid grain. B) SEM image of chloritoid grain with marked EMP measuring pattern, and associated diagram of the measured profile with X_{Mg} values across the chloritoid grain, on the right.

for the ratios La/Sc (1.85 – 5.43), Th/Sc (0.68 – 2.83), La/Co (1.20 – 7.41), and Th/Co (0.36 – 3.86) in the studied samples are indicative of dominantly felsic rock compositions in the source area of the protoliths of the studied metasediments (BHATIA & CROOK, 1986; CULLERS, 1994a,b; 2000) (Tab. 2). The La/Th versus Hf diagram (after FLOYD & LEVERIDGE, 1987) also indicates acidic arc rocks and a passive continental margin as a possible source for these protoliths (Fig. 11). Comparable conclusions can be drawn from the curves with similar tendencies of

HREE depletion on the spider diagram of REE concentrations in the studied rocks (normalized to chondrite, BOYNTON, 1984) (Fig. 4). Siliciclastic sediments coming from the mature continental crust are usually characterized by LREE enrichment and reasonably high and flat HREE values (CULLERS, 1994b; BALEN et al., 2013), which can be also seen in our samples (Fig. 4). In addition, pronounced negative Eu anomalies (Eu/Eu^*) ranging between 0.65 and 0.78 are consistent with those for siliciclastic sediments from felsic/granitoid sources (CULLERS, 2000,

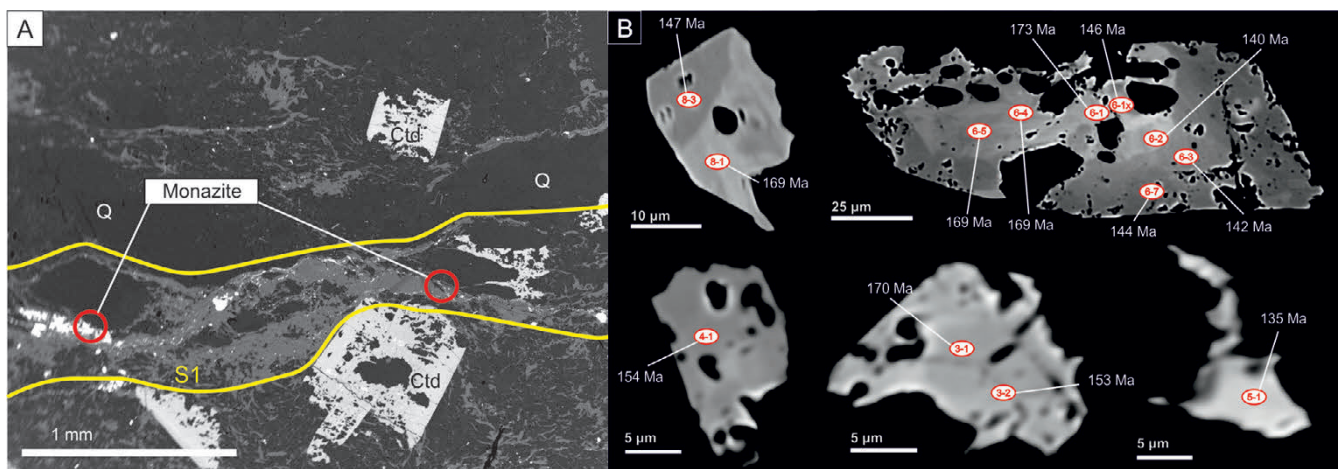


Figure 8. A) SEM-BSE image of objects in sample ST-6 with marked positions of the monazite grains, between the yellow lines is a cleavage domain (S1) composed of white mica and occasional metamorphic monazite (WM – white mica, Ctd – chloritoid, Q – quartz). B) SEM images of measured monazite grains with marked locations of the measurement spots (in red ellipse) and corresponding age data in white.

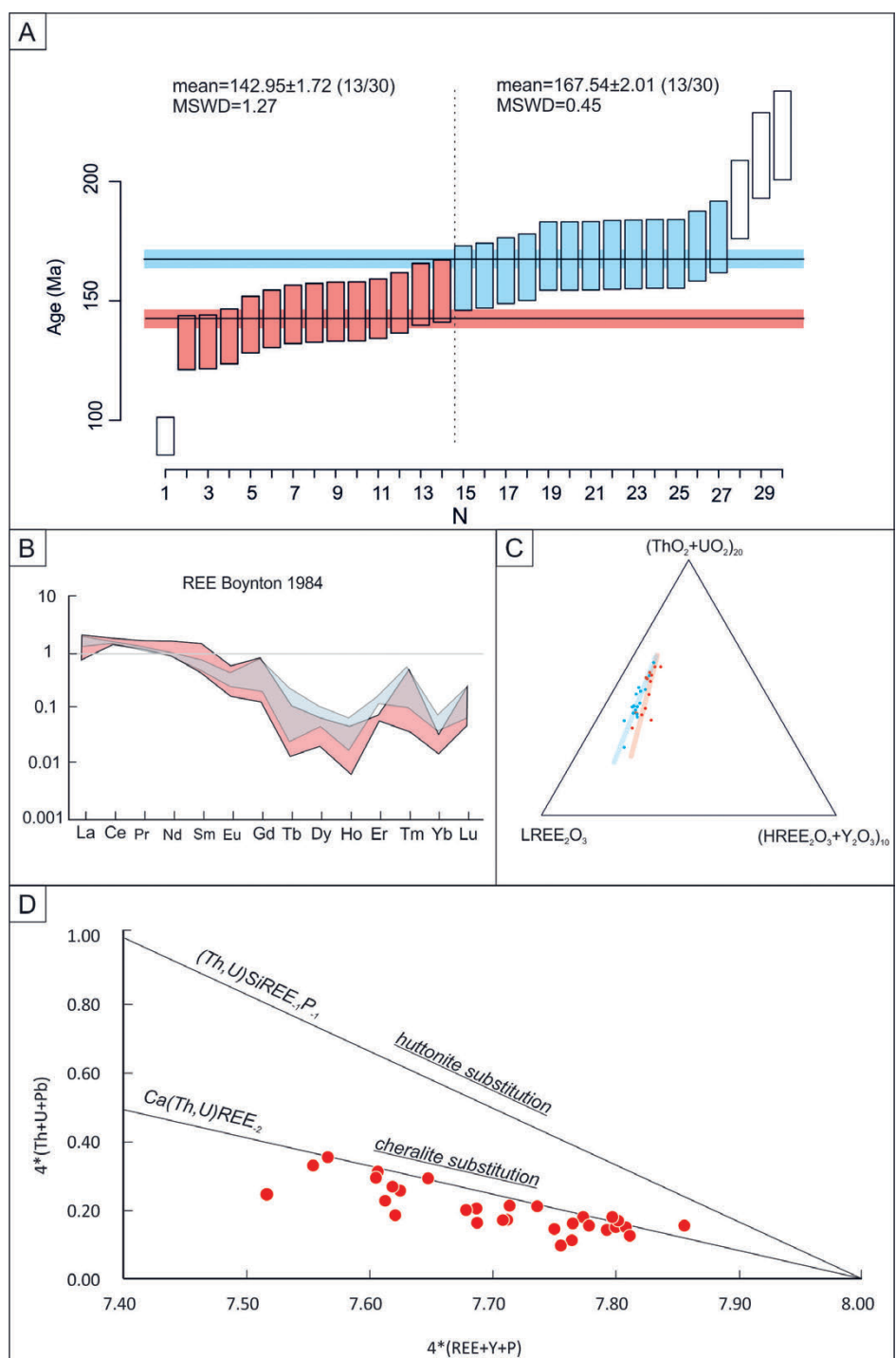


Figure 9. A) Diagram presenting the weighted mean of the two age groups determined on monazite, 142.95 Ma ($n=13$, in red) and 167.57 Ma ($n=13$, in blue), four measurements were excluded as outliers (transparent rectangles). B) chondrite REE pattern from monazite, sample ST-6 (REE in chondrite after BOYNTON, 1984). C) Triangular $\text{LREE}_2\text{O}_3 - (\text{ThO}_2 + \text{UO}_2)_{20} - (\text{HREE}_2\text{O}_3 + \text{Y}_2\text{O}_3)_{10}$ plot of monazite composition from sample ST-6, younger monazites (in red) and older monazite (in blue), trend lines are in the same colours (after ANDERSSON et al., 2018; SPEAR & PYLE, 2002). D) Diagram $4^*(\text{Th} + \text{U} + \text{Pb})$ vs. $4^*(\text{REE} + \text{Y} + \text{P})$ with exchange vectors; cheralite ($\text{Ca}(\text{Th}, \text{U})\text{REE}_2$ -2) in opposite to huttonite ($(\text{Th}, \text{U})\text{SiREE}_{-1}\text{P}_1$) for a sample of chloritoid schist (ST-6) Medvednica Mt. (after PYLE et al., 2001; ONDREJKA et al., 2012).

2002). The contents of trace elements in our rocks show similar patterns and agree well with the composition of the upper continental crust (MCLENNAN, 2001) (Fig. 4). According to the geochemical features of the studied schists (Tab. 2; Fig. 4), the detritus for their protoliths is predominantly upper crustal material with felsic rocks dominating in the source area. Similar conclusions can be drawn from analyses of metasediments from Medvednica Mt. by MIŠUR et al. (2013; 2015). The authors analysed a sample of chloritoid schist (D7 in Table 2) from the same locality

as in this study but taken from a lower position of the outcrop. The difference in REE contents between the here studied sample ST-6 and sample D7 is minor (Fig. 4) and can be prescribed to common variations of similar metasediments within an outcrop.

Based on lithological analogy, the age of detrital zircons and palaeontological analyzes of the surrounding rocks, the chloritoid schist protolith sediment was deposited during the Upper Permian-Lower Triassic or younger (ĐURĐANOVIĆ, 1973; BELAK 2005; MIŠUR, 2017; BELAK et al., 2022).

Table 4. Representative electron microprobe analyses of monazite composition, U, Th, Pb, REE and calculated forming ages, from chloritoid schist ST-6 (Medvednica Mt.). The structural formulae are calculated based on 16 oxygen atoms (in atoms per formula unit, apfu). Calculated ages (at the bottom) and selected chemical data (REEs, Y, Th, U, Pb normalized to chondrite after BOYNTON, 1984). The younger monazite age group is highlighted in pale grey; dark grey refers to the older monazite group.

Monazite	mnz l/1	mnz 3/4	mnz B/2	mnz 5/1	mnz 6/2	mnz 6/3	mnz 6/7	mnz B/1	mnz E/7	mnz 6/1x	mnz 8/3	mnz 3/5	mnz 3/2	mnz 4/1	mnz 3/2x
SiO ₂	0.29	0.48	0.29	0.37	0.67	0.37	0.25	0.29	0.34	0.61	0.66	0.74	0.52	0.31	0.40
P ₂ O ₅	29.05	27.23	28.71	28.00	27.41	27.75	27.92	28.40	28.99	27.40	27.28	27.04	27.70	28.46	28.03
As ₂ O ₅	0.02	0.00	0.00	0.00	0.02	0.07	0.00	0.05	0.01	0.02	0.01	0.00	0.00	0.00	0.00
PbO	0.01	0.03	0.02	0.03	0.04	0.02	0.02	0.02	0.02	0.04	0.03	0.03	0.03	0.02	0.02
ThO ₂	2.18	4.58	3.21	4.52	5.89	3.78	2.76	2.87	2.86	5.67	4.98	4.55	4.98	2.72	2.84
UO ₂	0.02	0.05	0.03	0.07	0.05	0.03	0.03	0.04	0.03	0.04	0.06	0.04	0.05	0.04	0.04
Y ₂ O ₃	0.45	0.66	0.59	0.65	0.85	0.83	0.54	0.57	0.56	0.67	0.64	0.55	0.68	1.62	0.37
La ₂ O ₃	13.17	11.88	12.54	13.02	4.60	4.96	9.99	12.65	14.56	8.21	11.09	13.45	11.86	9.59	14.17
Ce ₂ O ₃	31.06	32.12	29.17	29.67	22.67	23.61	32.03	30.21	33.41	29.73	31.81	30.56	31.86	31.61	31.13
Pr ₂ O ₃	3.32	3.53	3.31	3.35	4.08	4.16	3.83	3.32	3.24	3.85	3.57	3.29	3.50	3.94	3.27
Nd ₂ O ₃	12.45	13.40	13.72	13.15	20.37	21.23	15.57	13.54	11.77	16.04	13.49	13.08	13.31	15.45	12.16
Sm ₂ O ₃	2.58	2.20	3.25	2.54	6.15	6.36	2.85	3.10	1.95	3.07	2.29	2.25	2.21	2.64	2.16
Eu ₂ O ₃	0.57	0.36	0.72	0.55	1.00	0.95	0.46	0.69	0.28	0.53	0.30	0.33	0.32	0.46	0.45
Gd ₂ O ₃	3.90	0.92	4.91	1.51	3.17	3.03	1.76	4.73	3.74	1.85	0.78	1.22	0.89	1.49	1.46
Tb ₂ O ₃	0.05	0.00	0.12	0.12	0.11	0.12	0.07	0.10	0.02	0.11	0.05	0.08	0.05	0.08	0.09
Dy ₂ O ₃	0.24	0.22	0.40	0.39	0.51	0.48	0.34	0.38	0.16	0.31	0.17	0.23	0.22	0.29	0.21
Ho ₂ O ₃	0.06	0.00	0.00	0.00	0.04	0.05	0.00	0.00	0.01	0.06	0.08	0.03	0.05	0.04	0.00
Er ₂ O ₃	0.39	0.31	0.41	0.33	0.34	0.30	0.32	0.37	0.40	0.32	0.33	0.31	0.38	0.30	0.30
Tm ₂ O ₃	0.34	0.09	0.40	0.10	0.13	0.03	0.11	0.40	0.25	0.12	0.08	0.08	0.08	0.08	0.11
Yb ₂ O ₃	0.13	0.08	0.12	0.17	0.14	0.16	0.14	0.14	0.12	0.13	0.15	0.13	0.13	0.18	0.11
Lu ₂ O ₃	0.07	0.05	0.15	0.07	0.10	0.05	0.04	0.13	0.20	0.08	0.05	0.09	0.14	0.12	0.09
FeO	0.05	0.60	0.07	0.88	0.07	0.04	0.09	0.13	0.06	0.10	0.51	0.58	0.55	0.03	0.04
SO ₃	0.12	0.68	0.16	0.09	0.10	0.25	0.19	0.13	0.22	0.09	0.10	0.05	0.12	0.11	0.26
CaO	0.53	1.10	0.84	0.98	0.99	0.98	0.73	0.68	0.75	0.83	0.77	0.60	0.80	0.65	0.86
SrO	0.10	0.42	0.12	0.17	0.07	0.06	0.08	0.13	0.10	0.07	0.06	0.03	0.07	0.05	0.16
Al ₂ O ₃	0.01	0.00	0.00	0.00	0.00	0.00	0.00	0.00	0.00	0.00	0.00	0.00	0.00	0.00	0.01
Total	101.18	100.97	103.28	100.71	99.55	99.67	100.09	103.08	104.05	99.95	99.30	99.34	100.50	100.25	98.72
Si	0.05	0.08	0.04	0.06	0.11	0.06	0.04	0.05	0.05	0.10	0.11	0.12	0.08	0.05	0.06
P	3.88	3.68	3.81	3.79	3.78	3.80	3.81	3.79	3.80	3.77	3.76	3.74	3.77	3.84	3.83
As	0.00	0.00	0.00	0.00	0.00	0.01	0.00	0.00	0.00	0.00	0.00	0.00	0.00	0.00	0.00
Pb	0.00	0.00	0.00	0.00	0.00	0.00	0.00	0.00	0.00	0.00	0.00	0.00	0.00	0.00	0.00
Th	0.08	0.17	0.11	0.16	0.22	0.14	0.10	0.10	0.10	0.21	0.18	0.17	0.18	0.10	0.10
U	0.00	0.00	0.00	0.00	0.00	0.00	0.00	0.00	0.00	0.00	0.00	0.00	0.00	0.00	0.00
Y	0.04	0.06	0.05	0.05	0.07	0.07	0.05	0.05	0.05	0.06	0.06	0.05	0.06	0.14	0.03
La	0.77	0.70	0.73	0.77	0.28	0.30	0.59	0.74	0.83	0.49	0.67	0.81	0.70	0.56	0.84
Ce	1.79	1.88	1.67	1.74	1.35	1.40	1.89	1.74	1.90	1.77	1.90	1.83	1.88	1.85	1.84
Pr	0.19	0.21	0.19	0.20	0.24	0.25	0.23	0.19	0.18	0.23	0.21	0.20	0.21	0.23	0.19
Nd	0.70	0.76	0.77	0.75	1.18	1.23	0.90	0.76	0.65	0.93	0.78	0.76	0.76	0.88	0.70
Sm	0.14	0.12	0.18	0.14	0.35	0.36	0.16	0.17	0.10	0.17	0.13	0.13	0.12	0.15	0.12
Eu	0.03	0.02	0.04	0.03	0.06	0.05	0.03	0.04	0.01	0.03	0.02	0.02	0.02	0.03	0.02
Gd	0.20	0.05	0.26	0.08	0.17	0.16	0.09	0.25	0.19	0.10	0.04	0.07	0.05	0.08	0.08
Tb	0.00	0.00	0.01	0.01	0.01	0.01	0.00	0.01	0.00	0.01	0.00	0.00	0.00	0.00	0.00
Dy	0.01	0.01	0.02	0.02	0.03	0.03	0.02	0.02	0.01	0.02	0.01	0.01	0.01	0.01	0.01
Ho	0.00	0.00	0.00	0.00	0.00	0.00	0.00	0.00	0.00	0.00	0.00	0.00	0.00	0.00	0.00
Er	0.02	0.02	0.02	0.02	0.02	0.02	0.02	0.02	0.02	0.02	0.02	0.02	0.02	0.02	0.02
Tm	0.02	0.00	0.02	0.01	0.01	0.00	0.01	0.02	0.01	0.01	0.00	0.00	0.00	0.00	0.01
Yb	0.01	0.00	0.01	0.01	0.01	0.01	0.01	0.01	0.01	0.01	0.01	0.01	0.01	0.01	0.01
Lu	0.00	0.00	0.01	0.00	0.01	0.00	0.00	0.01	0.01	0.00	0.00	0.00	0.01	0.01	0.00
Fe ²⁺	0.01	0.08	0.01	0.12	0.01	0.01	0.01	0.02	0.01	0.01	0.07	0.08	0.07	0.00	0.01
S	0.01	0.08	0.02	0.01	0.01	0.03	0.02	0.02	0.03	0.01	0.01	0.01	0.01	0.01	0.03
Ca	0.09	0.19	0.14	0.17	0.17	0.17	0.13	0.11	0.13	0.14	0.13	0.10	0.14	0.11	0.15
Sr	0.01	0.04	0.01	0.02	0.01	0.01	0.01	0.01	0.01	0.01	0.01	0.00	0.01	0.00	0.01
Al	0.00	0.00	0.00	0.00	0.00	0.00	0.00	0.00	0.00	0.00	0.00	0.00	0.00	0.00	0.00
X(cheralite)	0.04	0.09	0.07	0.08	0.08	0.08	0.06	0.06	0.06	0.07	0.06	0.05	0.07	0.05	0.07
X(huttonite)	0.00	0.00	0.00	0.00	0.01	0.00	0.00	0.00	0.00	0.02	0.01	0.02	0.01	0.00	0.00
X(monazite)	0.96	0.91	0.94	0.92	0.90	0.92	0.95	0.95	0.95	0.91	0.92	0.93	0.92	0.95	0.94
Sum Kat.	8.06	8.15	8.11	8.15	8.09	8.09	8.10	8.12	8.10	8.09	8.12	8.13	8.12	8.08	8.08
Age (Ma)	93.30	132.50	132.80	135.10	140.10	142.50	144.40	145.00	145.50	145.60	146.80	149.20	152.80	154.10	159.60
2 sd	8.10	11.50	11.50	11.70	12.10	12.30	12.50	12.60	12.60	12.60	12.70	12.90	13.20	13.30	13.80

Table 4. (continued)

Monazite	mnz E/1	mnz 1/2	mnz E/6	mnz 6/5	mnz F/1	mnz 8/1	mnz 6/4	mnz 1/3	mnz 3/1	mnz B/3	mnz 6/1	mnz 3/6	mnz 3/1x	mnz C/1	mnz 2/1
SiO ₂	0.36	0.43	0.51	0.37	0.27	0.43	0.39	0.17	0.48	0.35	0.37	0.82	0.26	0.29	0.47
P ₂ O ₅	28.75	27.69	28.80	27.70	28.90	28.79	27.72	28.07	27.50	28.72	27.61	26.68	27.81	28.94	27.40
As ₂ O ₅	0.00	0.00	0.00	0.07	0.00	0.03	0.00	0.01	0.00	0.00	0.00	0.00	0.00	0.00	0.00
PbO	0.02	0.03	0.02	0.02	0.01	0.03	0.03	0.02	0.04	0.02	0.02	0.05	0.03	0.03	0.03
ThO ₂	2.73	3.85	2.77	3.20	1.56	3.73	3.99	2.29	4.80	3.16	2.71	5.78	3.46	2.80	2.98
UO ₂	0.03	0.03	0.06	0.04	0.03	0.04	0.04	0.03	0.05	0.03	0.08	0.04	0.04	0.04	0.03
Y ₂ O ₃	0.62	0.61	0.42	0.69	0.43	0.66	0.64	0.53	0.66	0.35	0.46	0.60	0.35	0.55	0.30
La ₂ O ₃	14.99	12.84	15.00	11.62	13.69	11.57	11.38	15.29	11.78	13.56	12.14	10.60	15.08	13.47	13.28
Ce ₂ O ₃	31.76	32.54	30.55	32.36	31.65	32.38	32.23	34.08	31.79	31.50	29.36	30.69	31.37	32.54	31.24
Pr ₂ O ₃	3.38	3.51	3.31	3.71	3.47	3.59	3.76	3.35	3.48	3.38	3.40	3.61	3.18	3.43	3.56
Nd ₂ O ₃	12.62	12.75	12.99	14.22	13.21	13.93	14.29	11.43	13.24	12.96	13.84	13.78	11.59	12.69	13.28
Sm ₂ O ₃	2.34	2.14	2.64	2.26	2.86	2.33	2.39	1.71	2.17	2.69	2.93	2.34	2.03	2.27	2.59
Eu ₂ O ₃	0.35	0.34	0.51	0.33	0.58	0.38	0.34	0.26	0.31	0.51	0.57	0.37	0.37	0.35	0.45
Gd ₂ O ₃	3.84	0.92	4.30	1.02	4.50	0.95	1.11	0.71	0.93	4.34	1.97	1.18	1.34	3.74	1.71
Tb ₂ O ₃	0.03	0.01	0.06	0.06	0.05	0.06	0.07	0.00	0.06	0.09	0.15	0.09	0.07	0.02	0.06
Dy ₂ O ₃	0.22	0.11	0.18	0.26	0.31	0.15	0.30	0.12	0.23	0.20	0.38	0.32	0.18	0.20	0.31
Ho ₂ O ₃	0.01	0.00	0.05	0.01	0.00	0.00	0.00	0.00	0.03	0.00	0.00	0.00	0.02	0.02	0.05
Er ₂ O ₃	0.43	0.34	0.39	0.33	0.38	0.34	0.35	0.31	0.36	0.39	0.29	0.30	0.32	0.40	0.34
Tm ₂ O ₃	0.36	0.04	0.32	0.12	0.36	0.06	0.14	0.05	0.08	0.39	0.07	0.09	0.06	0.34	0.06
Yb ₂ O ₃	0.11	0.10	0.14	0.15	0.13	0.08	0.16	0.08	0.11	0.17	0.13	0.10	0.12	0.12	0.15
Lu ₂ O ₃	0.12	0.02	0.03	0.06	0.10	0.09	0.08	0.10	0.12	0.08	0.05	0.10	0.12	0.16	0.12
FeO	0.00	0.50	0.02	0.10	0.62	0.41	0.18	0.48	0.61	0.10	0.16	0.50	0.00	0.69	0.26
SO ₃	0.04	0.09	0.11	0.13	0.48	0.10	0.10	0.35	0.13	0.10	0.36	0.07	0.28	0.18	0.62
CaO	0.45	0.57	0.58	0.63	0.84	0.64	0.68	0.76	0.82	0.60	0.88	0.68	0.91	0.77	1.09
SrO	0.04	0.05	0.07	0.05	0.19	0.06	0.06	0.09	0.08	0.08	0.20	0.05	0.16	0.08	0.44
Al ₂ O ₃	0.00	0.01	0.01	0.00	0.02	0.00	0.00	0.00	0.00	0.00	0.04	0.00	0.00	0.00	0.02
Total	103.61	99.49	103.83	99.50	104.66	100.83	100.43	100.27	99.85	103.77	98.16	98.82	99.13	104.09	100.82
Si	0.06	0.07	0.08	0.06	0.04	0.07	0.06	0.03	0.08	0.05	0.06	0.14	0.04	0.04	0.07
P	3.81	3.80	3.80	3.80	3.76	3.85	3.79	3.80	3.77	3.81	3.80	3.72	3.81	3.80	3.71
As	0.00	0.00	0.00	0.01	0.00	0.00	0.00	0.00	0.00	0.00	0.00	0.00	0.00	0.00	0.00
Pb	0.00	0.00	0.00	0.00	0.00	0.00	0.00	0.00	0.00	0.00	0.00	0.00	0.00	0.00	0.00
Th	0.10	0.14	0.10	0.12	0.05	0.13	0.15	0.08	0.18	0.11	0.10	0.22	0.13	0.10	0.11
U	0.00	0.00	0.00	0.00	0.00	0.00	0.00	0.00	0.00	0.00	0.00	0.00	0.00	0.00	0.00
Y	0.05	0.05	0.03	0.06	0.03	0.06	0.05	0.04	0.06	0.03	0.04	0.05	0.03	0.05	0.03
La	0.87	0.77	0.86	0.69	0.78	0.67	0.68	0.90	0.70	0.78	0.73	0.64	0.90	0.77	0.78
Ce	1.82	1.93	1.74	1.92	1.78	1.87	1.90	1.99	1.88	1.80	1.75	1.85	1.86	1.85	1.83
Pr	0.19	0.21	0.19	0.22	0.19	0.21	0.22	0.20	0.21	0.19	0.20	0.22	0.19	0.19	0.21
Nd	0.71	0.74	0.72	0.82	0.73	0.79	0.82	0.65	0.77	0.72	0.80	0.81	0.67	0.70	0.76
Sm	0.13	0.12	0.14	0.13	0.15	0.13	0.13	0.09	0.12	0.15	0.16	0.13	0.11	0.12	0.14
Eu	0.02	0.02	0.03	0.02	0.03	0.02	0.02	0.01	0.02	0.03	0.03	0.02	0.02	0.02	0.02
Gd	0.20	0.05	0.22	0.05	0.23	0.05	0.06	0.04	0.05	0.23	0.11	0.06	0.07	0.19	0.09
Tb	0.00	0.00	0.00	0.00	0.00	0.00	0.00	0.00	0.00	0.00	0.01	0.00	0.00	0.00	0.00
Dy	0.01	0.01	0.01	0.01	0.02	0.01	0.02	0.01	0.01	0.01	0.02	0.02	0.01	0.01	0.02
Ho	0.00	0.00	0.00	0.00	0.00	0.00	0.00	0.00	0.00	0.00	0.00	0.00	0.00	0.00	0.00
Er	0.02	0.02	0.02	0.02	0.02	0.02	0.02	0.02	0.02	0.02	0.01	0.02	0.02	0.02	0.02
Tm	0.02	0.00	0.02	0.01	0.02	0.00	0.01	0.00	0.00	0.02	0.00	0.00	0.00	0.02	0.00
Yb	0.01	0.00	0.01	0.01	0.01	0.00	0.01	0.00	0.01	0.01	0.01	0.00	0.01	0.01	0.01
Lu	0.01	0.00	0.00	0.00	0.00	0.00	0.00	0.00	0.01	0.00	0.00	0.01	0.01	0.01	0.01
Fe ²⁺	0.00	0.07	0.00	0.01	0.08	0.05	0.02	0.06	0.08	0.01	0.02	0.07	0.00	0.09	0.03
S	0.01	0.01	0.01	0.02	0.06	0.01	0.01	0.04	0.02	0.01	0.04	0.01	0.03	0.02	0.07
Ca	0.07	0.10	0.10	0.11	0.14	0.11	0.12	0.13	0.14	0.10	0.15	0.12	0.16	0.13	0.19
Sr	0.00	0.00	0.01	0.00	0.02	0.01	0.01	0.01	0.01	0.01	0.02	0.00	0.01	0.01	0.04
Al	0.00	0.00	0.00	0.00	0.00	0.00	0.00	0.00	0.00	0.00	0.01	0.00	0.00	0.00	0.00
X(cheralite)	0.04	0.05	0.05	0.05	0.07	0.05	0.06	0.06	0.07	0.05	0.08	0.06	0.08	0.06	0.09
X(buttonite)	0.01	0.01	0.00	0.00	0.01	0.01	0.00	0.01	0.01	0.00	0.00	0.02	0.00	0.00	0.00
X(monazite)	0.96	0.94	0.95	0.94	0.95	0.94	0.94	0.95	0.92	0.95	0.94	0.92	0.93	0.94	0.93
Sum Kat.	8.10	8.11	8.10	8.10	8.15	8.07	8.11	8.12	8.13	8.10	8.10	8.12	8.09	8.14	8.15
Age (Ma)	160.60	162.70	164.10	168.80	168.80	168.90	169.30	169.50	169.70	169.70	173.00	176.80	192.50	211.00	219.40
2 sd	13.90	14.10	14.20	14.60	14.60	14.60	14.70	14.70	14.70	14.70	15.00	15.30	16.70	18.30	19.00

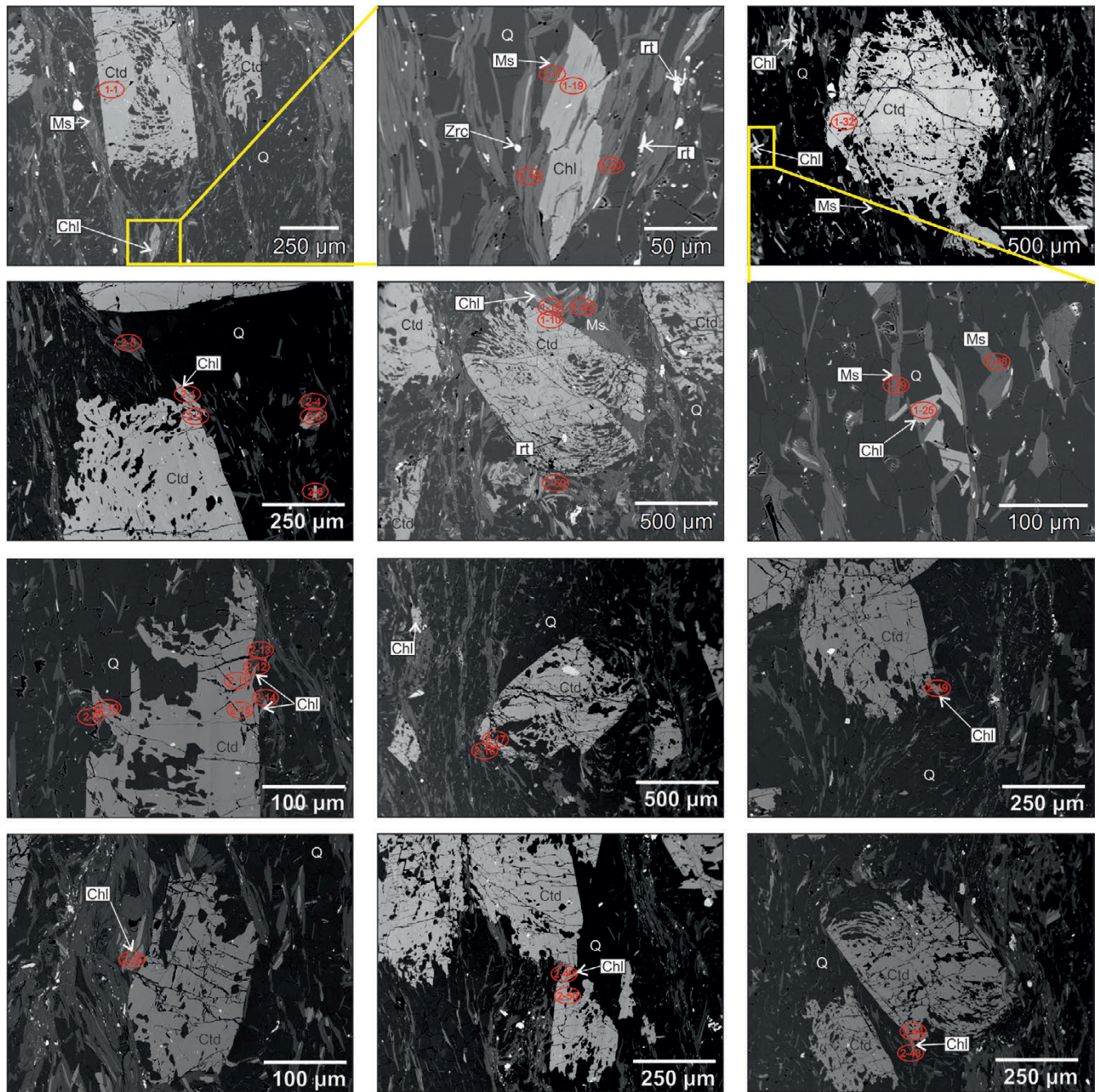


Figure 10. Table with SEM images of chloritoid schist from Medvednica Mt. The red ellipses indicate the position and names of EMP measurements of chlorite (Chl), chloritoid (Ctd), muscovite (Ms), rutile (rt), zircon (Zrc) and quartz (Q) (for results of measurements see Tables 3 and 5).

5.2. Metamorphic evolution

The mineralogical characteristics of the sample ST-6 (chloritoid porphyroblasts with textural sector-hourglass zoning, hypidiomorphic chlorite blasts, synmetamorphic white micas) indicate metamorphic conditions of the greenschist to amphibolite facies. Similar results can be seen in published studies (e.g. MPOSKOS, 1989; BUCHER & GRAPES, 2011; CASTELLANOS-ALLARCÓN et al., 2016). The C'-type shear band cleavage structure in sample ST-6 points to specific ductile deformation mechanisms (Fig. 3C) (PASSCHIER & TROUW, 2005). The quartz grain boundaries formed by SGR and GBM processes (Fig. 3F) are usually associated with recrystallization temperatures ranging from 400 to 600 °C (STIPP et al., 2002). The two selected chloritoid blasts showed slight Mg enrichment and Mn depletion from the core towards the rim (Fig. 7A; B), which is a typical feature of

prograde metamorphism during the growth of chloritoid (e.g. MPOSKOS, 1989; SPEAR, 1995; FRANCESCHELLI & MEMMI, 1999; KOROKNAI et al., 2001).

If we consider the P-T pseudosection with 10% of Fe as Fe_2O_3 to be the most appropriate for our sample (see LO PÒ & BRAGA, 2014), the calculated fluid-free modal contents at these conditions are 78.7 vol% quartz, 13.1 vol% muscovite, 6.9 vol% chloritoid, 0.6 vol% chlorite, and 0.6 vol% ilmenite. Thermodynamic modelling yielded an overlap of the isopleths of XFe in chlorite, XFe in chloritoid, and Si in muscovite at peak metamorphic temperatures around 550 °C and pressures around 0.94 GPa (Fig. 12). This result is also compatible with the results of the applied thermometers (chlorite–chloritoid: 527 – 568 °C, chlorite: 250 – 598 °C, Tab. 5). The scatter of the chlorite thermometric results could be due to the high metamorphic temperature, which is not suitable

Table 5. Table with the results of the classic geobarometric calculations; geothermometer based on chloritoid – chlorite pairs (after VIDAL et al., 1999), chlorite geothermometer (after INOUE et al., 2018) and phengite geobarometer (after CADDICK & THOMPSON, 2008).

Chlorite-chloritoid geothermometry (VIDAL et al., 1999)										
Chlorite-chloritoid pairs										
Chlorite	1-15	1-19	1-25	2-12	2-49	2-9	2-14	2-43	2-1	2-16
Chloritoid	1-10	1-1	1-32	2-11	2-50	2-10	2-15	2-44	2-2	2-17
T (°C)	545	568	556	546	553	561	556	534	527	547
average 549 °C						min=	527	max=	568	
Chlorite thermometry (INOUE et al., 1999)										
Chlorite	1-18	1-23	1-27	1-30	1-46	1-48	1-53	2-6	2-38	2-19
T (°C)	598	363	385	400	331	452	411	424	365	370
Chlorite	2-25	2-41	2-45					min=	250	max=
T (°C)	321	579	250					max=	598	
Phengite barometry (CHADDICK & THOMPSON, 2008)										
Muscovite	1-11	1-12	1-16	1-17	1-20	1-28	1-29	1-50	1-52	min
T (°C)	P (GPa)									max
600	0.94	1.07	1.01	0.99	1.01	1.06	0.98	1.06	1.00	0.94
550	0.87	0.99	0.94	0.92	0.94	0.98	0.90	0.98	0.93	0.87
500	0.79	0.92	0.86	0.84	0.86	0.91	0.83	0.91	0.85	0.79
450	0.72	0.84	0.79	0.77	0.79	0.83	0.75	0.83	0.78	0.72
average 0.94 GPa										0.84

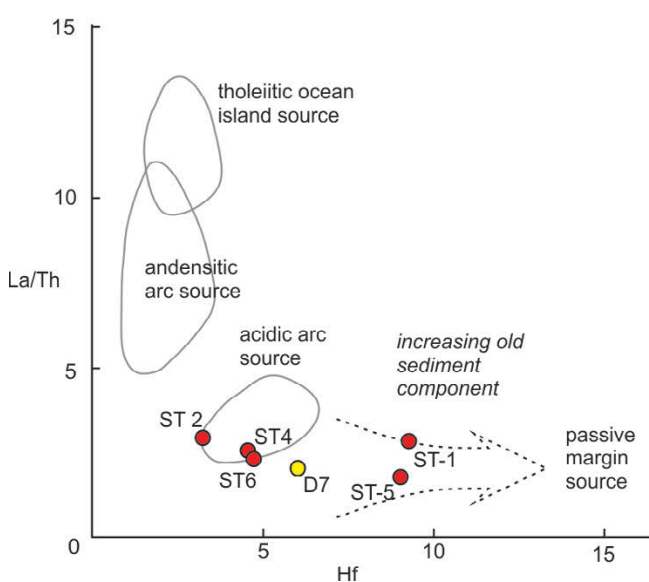
for precise chlorite thermometry (see VIDAL et al., 2016), and/or retrograde metamorphic reactions affecting chlorite. The geobarometry based on the Si content in muscovite (after CADDICK & THOMPSON, 2008) resulted in a pressure range from 0.87 to 0.99 GPa (at 550 °C, Tab. 5) which is also compatible with the modelling results. Hence, we suggest that the metamorphic peak conditions were determined fairly precisely at 0.94 ± 0.05 GPa and 550 ± 20 °C (Fig. 12). Based on petrographic observations and thermodynamic calculations, the main mineral reaction to form chloritoid in sample ST-6 is haematite + chlorite = magnetite + chloritoid + quartz + H₂O. This reaction was also formulated by BELAK et al. (1995a).

We note a considerable difference in the estimated P-T conditions for PMMC metasediments between our study and previous works (300 – 410 °C by the Kübler index method; medium pressure by the b₀ method, JUDIK et al., 2004; 2008; 300 – 350 °C by chlorite thermometry, LUGOVIC et al., 2006). The b₀ method applied to potassic white mica-bearing rocks of the PMMC (JUDIK et al., 2004) is highly dependent on the mineral assemblage (MASSONNE & SCHREYER, 1989; MASSONNE & SZPURKA, 1997) and local equilibrium. For example, a graphical presentation of whole rock and the <2 µm fraction sample data (Fig. 4 in JUDIK et al., 2004) shows scattering from low-, medium- to high-pressure ranges with maximum frequency distributions in the medium-pressure range which is later ascribed to the values of 0.3 – 0.4 GPa. The likely reason for such a difference is that the investigated chloritoid schist is part of a sequence located at a higher metamorphic grade in comparison to the rocks studied by JUDIK et al. (2004). The previous temperature estimates, based on the Kübler index (illite crystallinity), empirical chlorite thermometry and vitrinite reflectance, should be taken as semiquantitative, but the difference of more than 100 °C between our study and the previous works (JUDIK et al., 2004; 2008; LUGOVIC et al., 2006) cannot be a matter of the applied methods alone but also of the position in a metamorphic sequence. The temperature difference is considered to be broadly realistic and can be explained by a geodynamic scenario outlined in section 5.4.

5.3. Monazite dating

The investigated monazite grains are located in the cleavage domains (S₁), which are mainly composed of syn-metamorphic white mica (Fig. 8A). The U concentration in the investigated monazite is lower than 0.005 apfu (<0.0028 apfu) (Tab. 4), which is characteristic of metamorphic monazite (SPEAR & PYLE, 2002). The measured monazite is highly irregular in shape and of small dimension (<200 µm) (Fig. 8B) which is also a typical feature of monazite in upper greenschist- and amphibolite-facies rocks (PARRISH,

Figure 11. A discrimination diagram La/Th versus Hf for the investigated samples of metasediments from Medvednica Mt. in red circles, in the yellow circle is a sample (D7) from MIŠUR et al. (2013) (after FLOYD & LAVERIDGE, 1987).



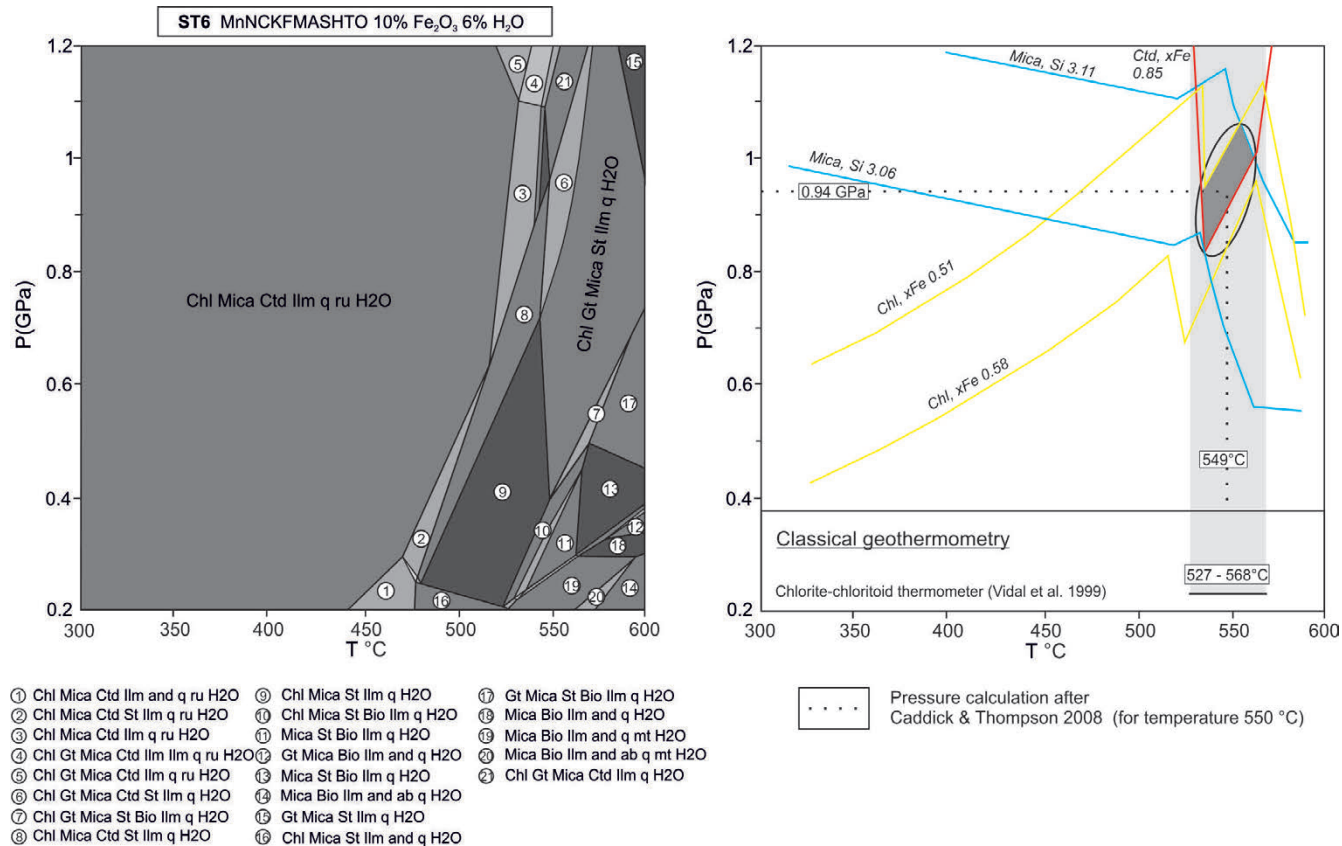


Figure 12. Pseudosection diagram calculated in the system MnNCKFMASHTO for sample ST-6, (PERPLE_X software package, CONNOLLY & PETRINI, 2002; CONNOLLY, 1990; 2005). The numbers in the circles refer to mineral assemblages given at the bottom. Abbreviations: and – andalusite; Bio – biotite; Ca – carpholite; Chl – chlorite; Ctd – chloritoid; Gt – garnet; Ilm – ilmenite; Mica – muscovite; St – stilpnomelane; ru – rutile; Q – quartz. Left hand side: calculated stability polygons with indicated mineral phases with legend below. Right hand side: graph with isopleths of chloritoid (red line), chlorite (yellow line) and muscovite (blue line). The dark grey polygon marks the intersection of the chlorite, chloritoid and muscovite isopleths. The diagram on the right hand side at the bottom presents the results of the classic thermobarometric calculations.

1990; FINGER & KRENN, 2007; SCHULZ, 2021). No obvious relationship between age data and the shape of monazite grains is recorded. The presence of two age domains even within single monazite crystals (see Tab 4, Fig. 8B, e.g.; grain mnz 6, mnz 3, mnz E, mnz B, mnz 8) indicates a two-phase growth (or possible recrystallization and/or fluid overprinting) of monazite at 143 ± 2 Ma and 167.5 ± 2 Ma. The HREE concentrations, followed by the Y₂O₃ values indicate slightly different trends between younger and older monazite populations (Tab. 4) with higher Y₂O₃ concentrations in the younger monazite domains (Fig. 9C). According to SCHULZ, (2021), this feature could be related to a higher metamorphic grade in forming the younger population, but the influence of other assemblage phases, particularly the presence of xenotime could discourage that conclusion. Nevertheless, the zonation of monazite indicates growth during different metamorphic phases (FRANZ et al., 1996; HEINRICH et al., 1997; SCHULZ, 2021).

Compared to previous Ar-Ar and K-Ar dating of white mica and whole-rock (110 – 122 Ma, BELAK et al., 1995a; 64 – 124 Ma, JUDIK et al., 2006; 122 – 135 Ma BOROJEVIĆ ŠOŠTARIĆ et al., 2012) our study yielded older ages. Even the oldest age from the literature is younger than the age of our young monazite group by about 8 Ma. The monazite U-Th total Pb dating method has been proven to be a robust dating method for metamorphic conditions (PARRISH, 1991; MONTEL et al., 1996; WILLIAMS et al., 2007; SCHULZ, 2021 and references therein), whereas the K-Ar and Ar-Ar, methods suffer from resetting during higher metamorphic conditions because of the limited thermal retentivity of micas and feldspars resulting in the overprint of older meta-

morphic records (PARRISH, 1991). Therefore, we assume that the previously published Cretaceous K-Ar and Ar-Ar ages represent cooling ages relevant to retrograde metamorphic conditions of the complex (e.g., ~300°C, according to VAN GELDER et al., 2015) which is also suggested by JUDIK et al. (2004).

5.4. Geodynamic interpretation

It is a common view that the opening and extension of the Neo-tethys ocean between the Tisia and Adria microplates was followed by intra-oceanic subduction during which one part of the Neotethys ocean was subducted (BABIC et al., 2002; PAMIĆ, 2002; KARAMATA, 2006; SCHMID et al., 2008; 2020). Subsequently, as a consequence of the shortening and subduction (i.e. closure of the ocean realm), a part of the oceanic crust collided and was obducted onto the CMA to form ophiolites (LUGOVIĆ et al., 2006; SCHMID et al., 2008; 2020). It is possible that part of the CMA, along with the oceanic Neotethys crust, was subducted beneath the accretion melâne (Middle Jurassic-Early Cretaceous), and eventually, during subsequent divergence, exhumed to the surface along with thin parts of oceanic crust (see PORKOLÁB et al., 2021). PORKOLÁB et al. (2021) published numerical models of continental crust subducted beneath an oceanic plate utilizing thermo-mechanical simulations and the data from ophiolite belts around the world. In these models, the subducted continental crust, driven by buoyancy, extrudes along with fragments of the oceanic plate. A similar situation was described for the Oman ophiolite region as a trench-passive margin (see ROBERTSON, 2004; and references therein). Part of the con-

tinental crust (Arabian plate) along with the oceanic Neotethys crust was subducted under an accretion melâne until its thickened wedge prevented further subduction and was followed by buoyancy-driven exhumation (ROBERTSON, 2004). The Oman-type trench-passive margin collision model is widely applicable to the Eastern Mediterranean region and explains the emplacement of most of the Jurassic and Cretaceous ophiolites onto former passive margins (ROBERTSON, 2004).

If we apply the above model to the part of the CMA that was subducted to depths of 35 – 38 km (0.94 GPa) and heated up to 550 °C according to the investigated chloritoid schist, this part would have been originally located close to the sole of the hot ophiolite that was later obducted. Metasediments of the PMMC that had experienced lower temperatures (300 – 410 °C) could have been not so deeply subducted with the consequence that their peak pressures were also lower.

The age of the older monazite group (ca. 167.5 Ma) of the studied chloritoid schist, should then be related to the metamorphic event caused by the subduction of an external part of the CMA below the oceanic lithosphere. This age is consistent with those interpreted so far, referring to regional processes related to the Adria-Europe subduction margin during the Middle Jurassic (e.g. LANPHERE et al., 1975; ages from 160 – 170 Ma, OKR-USCH et al., 1978; ages from 161 – 169 Ma; DIMO-LAHITTE et al., 2001; ages from 160 – 174 Ma; SCHMID et al., 2008; 2020; ŠEGVIĆ et al., 2014; 2019; 2020; ages from 160 – 162 Ma; BELAK et al., 2022; ages from 150 – 165 Ma). The younger monazite group (143 Ma) could be related to the obduction process which included parts of the subducted CMA along with parts of the oceanic crust (LUGOVIĆ et al., 2006). In the model of PORKOLÁB et al. (2021), subduction and exhumation cycles usually last about 10 to 30 Ma, which would agree with the difference in age of our monazite groups.

6. CONCLUSIONS

The investigated chloritoid schist from Medvednica Mt. originated by metamorphism of clastic sediment accumulated at the edge of the CMA. Peak metamorphic conditions of 0.94 ± 0.05 GPa and 550 ± 20 °C were estimated by applying pseudosection modelling and classical geothermobarometry. The formation of metamorphic monazite in the studied chloritoid schist occurred at 167 ± 2 Ma and 143 ± 2 Ma. The ages are interpreted to correspond to two distinct metamorphic episodes. The metamorphic changes in the investigated rocks are initiated by regional subduction-accretion tectonics, synchronous with regional processes of the West Vardar ophiolite obduction onto the CMA during the Late Jurassic.

ACKNOWLEDGMENT

We would like to thank the personnel from the laboratory for sample preparation of the Croatian Geological Survey for the support that enabled this research. Support by the Croatian Science Foundation (IP-2014-09-9541) and by the Croatian Ministry of Science, Education, and Sports within the frame of the grant no. 181-1811096-1093 is acknowledged. We would also like to thank Andrea MIŠUR, Marko ŠPELIĆ and Marija HORVAT for their valuable suggestions in preparing the manuscript.

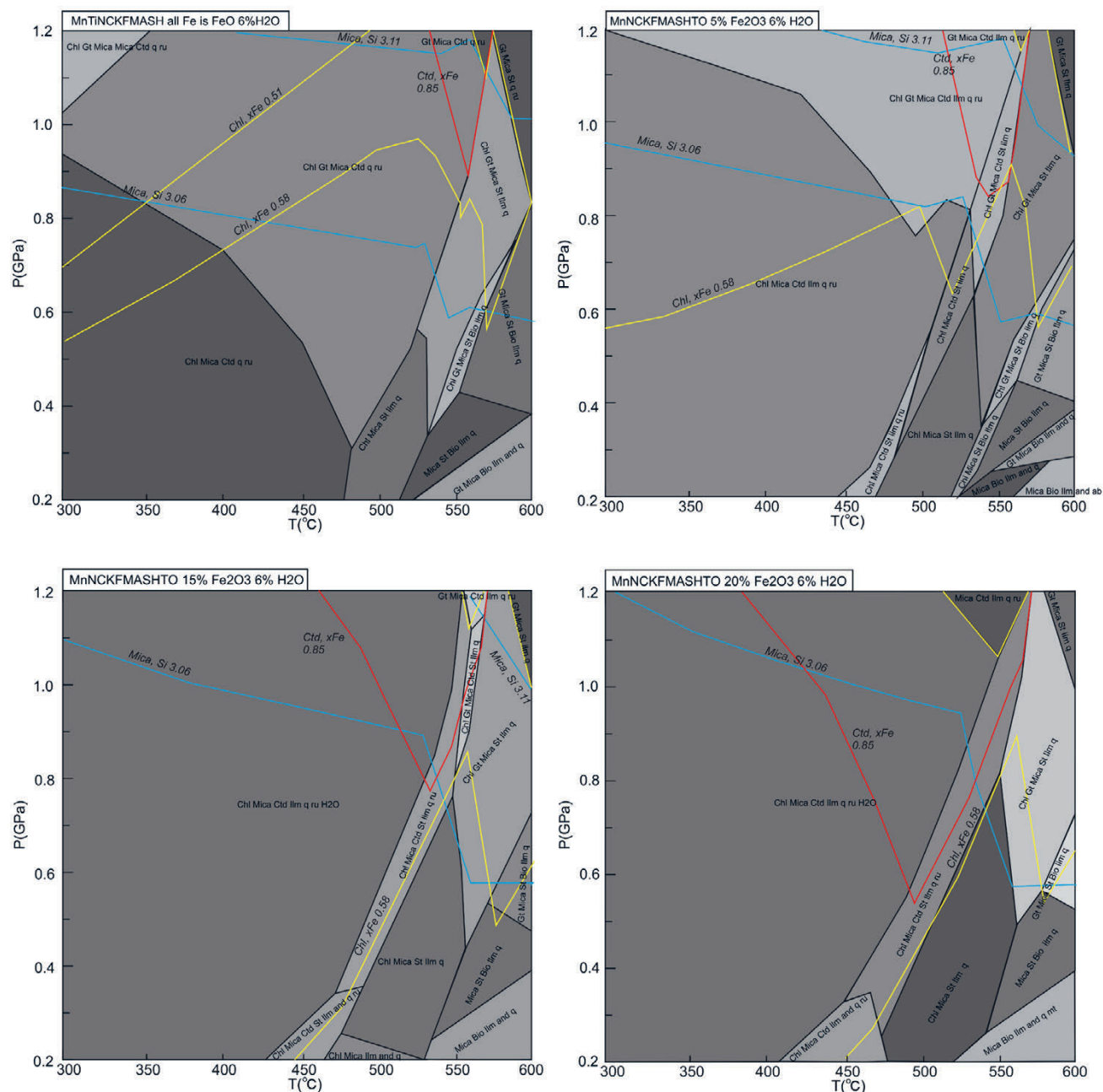
REFERENCES

- ABD ELMOLA, A., CHARPENTIER, D., BUATIER, M., LANARI, P. & MONIÉ, P. (2017): Textural-chemical changes and deformation conditions registered by phyllosilicates in a fault zone (Pic de Port Vieux thrust, Pyrenees).— Applied Clay Science, 144, 88–103. doi: 10.1016/j.clay.2017.05.008.
- ANDERSSON, S.S., WAGNER, T., JONSSON, E. & MICHALLIK, R.M. (2018): Mineralogy, paragenesis, and mineral chemistry of REEs in the Olserum-Djupedal REE-phosphate mineralization, SE Sweden.— American Mineralogist, 103, 125–142. doi: 10.2138/am-2018-6202
- ARBIOL, C., LAYNE, G.D., ZANONI, G. & ŠEGVIĆ, B. (2021): Characteristics and genesis of phyllosilicate hydrothermal assemblages from Neoproterozoic epithermal Au-Ag mineralisation of the Avalon Zone of Newfoundland, Canada.— Applied Clay Science, 202, 105960. doi: 10.1016/j.clay.2020.105960
- BABIĆ, Lj., HOCHULI, P.A. & ZUPANIĆ, J. (2002): The Jurassic ophiolitic mélange in the NE Dinarides: Dating, internal structure and geotectonic implications.— Eclogae Geologicae Helvetiae, 95, 263–275. doi: 10.5169/seals-168959
- BAILEY, S.W. (1980): Summary of recommendations of AIPEA nomenclature committee on clay minerals.— American Mineralogist, 65, 1–7.
- BALEN, D., HORVÁTH, P., FINGER, F. & STARIJAS, B. (2013): Phase equilibrium, geothermobarometric and xenotime age dating constrains on the Alpine metamorphism recorded in chloritoid schists from the southern part of the Tisia Mega-Unit (Slavonian Mts., NE Croatia).— International Journal of Earth Sciences., 102/4, 1091–1109. doi: 10.1007/s00531-012-0850-8
- BASCH, O. (1983a): Osnovna geološka karta SFRJ 1:100.000, list Ivanić-Grad L33-81 [Basic Geological Map of SFRY 1:100000, Ivanić-Grad sheet – in Croatian].— Geološki zavod, Zagreb, Savezni geološki zavod, Beograd.
- BASCH, O. (1983b): Osnovna geološka karta SFRJ 1:100.000, Tumač za list Ivanić-Grad [Basic Geological Map of SFRY 1:100000, Geology of the Ivanić-Grad sheet – in Croatian].— Geološki zavod, Zagreb, Savezni geološki zavod, Beograd, 81 p.
- BELAK, M. (2005): Metamorfne stijene plavih i zelenih skriljavaca na Medvednici [Metamorphic rocks of the blueschist and greenschist on the Medvednica Mt. – in Croatian, with an English Abstract].— Unpubl. PhD Thesis, Faculty of Science, University of Zagreb, 295 p.
- BELAK, M. & TIBLJAŠ, D. (1998): Discovery of the blueschist in the Medvednica Mountain (Northern Croatia) and their significance for the interpretation of the geotectonic evolution of the area.— Geologija Croatica, 51/1, 27–32. doi: 10.4154/GC.199/05
- BELAK, M., PAMIĆ, J., KOLAR-JURKOVŠEK, T., PECKAY, Z. & KARAN, D. (1995a): Alpinski regionalnometamorfni kompleks Medvednice (sjeverozapadna Hrvatska) [Alpine low-grade regional metamorphic complex of Mt. Medvednica northwestern Croatia – in Croatian].— In: VLAHOVIĆ, I. et al. (eds): 1st Croatian Geological Congress, Proceedings, 1, 67–70.
- BELAK, M., SREMAC, J., CRNKO, J. & KOLAR-JURKOVŠEK, T. (1995b): Paleozojske stijene niskog stupnja metamorfizma na jugoistočnoj strani Medvednice (sjeverozapadna Hrvatska) [Palaeozoic rocks of low metamorphic degree on the southeastern side of Medvednica (northwestern Croatia) – in Croatian].— In: VLAHOVIĆ, I. et al. (eds): 1st Croatian Geological Congress, Proceedings, 1, 71–74.
- BELAK, M., SLOVENEC, D., KOLAR-JURKOVŠEK, T., GARAŠIĆ, V., PÉCSKAY, Z., TIBLJAŠ, D & MIŠUR, I. (2022): Low-grade metamorphic rocks of the Tethys subduction–collision zone in the Medvednica Mt. (NW Croatia).— Geologica Carpathica, 73, 3, 207–229. doi: 10.31577/GeolCarp.73.3.3
- BHATIA, M.R. & CROOK, K.A.W. (1986): Trace element characteristics of greywackes and tectonic setting discrimination of sedimentary basins.— Contributions to Mineralogy and Petrology, 92, 181–193.
- BOYNTON, W.V. (1984): Geochemistry of the rare earth elements: meteorite studies.— In: HENDERSON, P. (ed.): Rare earth element geochemistry, Elsevier, Amsterdam, 63–114.
- BOROJEVIĆ ŠOSTARIĆ, S., NEUBAUER, F., ROBERT, H. & PALINKAŠ, A.L. (2012): Tectonothermal history of the basement rocks within the NW Dinarides: new $^{40}\text{Ar}/^{39}\text{Ar}$ Ages and synthesis.— Geologica Carpathica, 63, 441–452. doi: 10.2478/v10096-012-0034-2
- BUCHER, K. & GRAPES, R. (2011): Petrogenesis of Metamorphic Rocks.— Springer-Verlag Berlin Heidelberg, 419. doi: 10.1007/978-3-540-74169-5
- CADDICK, M.J. & THOMPSON, A.B. (2008): Quantifying the tectono-metamorphic evolution of pelitic rocks from a wide range of tectonic settings: mineral composition in equilibrium.— Contributions to Mineralogy and Petrology, 156, 177–195. doi: 10.1007/s00410-008-0280-6
- CAMILLERI, P.A. (2018): Classification, Character, and Origin of Textural Zoning in Porphyroblasts: Significance and Relation to Strain.— Journal of the Tennessee Academy of Science, 93, 1-2, 50–60.
- CASTELLANOS-ALARCÓN, O.M., RÍOS-REYES, C.A. & GARCÍA-RAMÍREZ, C.A. (2016): Occurrence of chloritoid-bearing metapelitic rocks and their significance in the metamorphism of the Silgará Formation at the Central Santander Massif.— Boletín de Ciencias de la Tierra, 40, 5–15. doi: 10.15446/rbct.n40.48416
- CHAUVENET, W. (1863): A Manual of Spherical and Practical Astronomy, Vol. 2.— J. B. Lippincott Company, Philadelphia, PA.
- CONNOLLY, J.A.D. (1990): Multivariable phase-diagrams— an algorithm based on generalised thermodynamics.— American Journal of Science, 290, 666–718.
- CONNOLLY, J.A.D. (2005): Computation of phase equilibria by linear programming: A tool for geodynamic modeling and its application to subduction zone decarbon-

- ation.– *Earth and Planetary Science Letters*, 236, 524–541. doi: 10.1016/j.epsl.2005.04.033
- CONNOLLY, J.A.D. & PETRINI, K. (2002): An automated strategy for calculation of phase diagram sections and retrieval of rock properties as a function of physical conditions.– *Journal of Metamorphic Geology*, 20/7, 697–708. doi: 10.1046/j.1525-1314.2002.00398.x
- CSONTOS, L. & NAGYMAROSY, A. (1998): The Mid-Hungarian line: a zone of repeated tectonic inversions.– *Tectonophysics*, 297/1, 51–71. doi: 10.1016/S0040-1951(98)00163-2
- CULLERS, R.L. (1994a): The chemical signature of source rocks in size fractions of Holocene stream sediment derived from metamorphic rocks in the Wet Mountains region, Colorado, USA.– *Chemical Geology*, 113, 327–343. doi: 10.1016/0009-2541(94)90074-4
- CULLERS, R.L. (1994b): The controls on the major and trace element variation of shales, siltstones, and sandstones of Pennsylvanian-Permian age from uplifted continental blocks in Colorado to platform sediment in Kansas, USA.– *Geochimica et Cosmochimica Acta*, 58, 4955–4972. doi: 10.1016/0016-7037(94)90224-0
- CULLERS, R.L. (2000): The geochemistry of shales, siltstones and sandstones of Pennsylvanian-Permian age, Colorado, USA: implications for provenance and metamorphic studies.– *Lithos*, 51, 181–203. doi: 10.1016/S0024-4937(99)0063-8
- CULLERS, R.L. (2002): Implications of elemental concentrations for provenance, redox conditions, and metamorphic studies of shales and limestones near Pueblo, CO, USA.– *Chemical Geology*, 191, 305–327. doi: 10.1016/S0009-2541(02)00133-X
- DIMO-LAHITTE, A., MONIE, P. & VERGELEY, P. (2001): Metamorphic soles from the Albanian ophiolites: Petrology, $^{40}\text{Ar}/^{39}\text{Ar}$ geochronology, and geodynamic evolution.– *Tectonics*, 20, 78–96. doi: 10.1029/2000TC900024
- ĐURDANOVIĆ, Ž. (1973): O paleozoiku i trijasu Medvednica (Zagrebačke gore) i područja Dvora na Uni na temelju konodonata [On the Palaeozoic and Triassic of Medvednica (Zagrebačke gora) and the Dvor na Una area based on conodonts (in Croatian)].– *Geološki vjesnik*, 25, 29–49.
- FINGER, F. & KRENN, E. (2007): Three metamorphic monazite generations in a high-pressure rock from the Bohemian Massif and the potentially important role of apatite in stimulating polyphase monazite growth along a PT loop.– *Lithos*, 95, 103–115. doi: 10.1016/j.lithos.2006.06.003
- FLOYD, P.A. & LEVERIDGE, B.E. (1987): Tectonic environment of the Devonian Gramscatho basin, south Cornwall: framework mode and geochemical evidence from turbiditic sandstones.– *Journal of the Geological Society of London*, 144, 531–542. doi: 10.1144/gsjgs.144.4.0531
- FODOR, L., JELEN, B., MÁRTON, E., SKABERNE, D., ČAR, J. & VRABEC, M. (1998): Miocene-Pliocene tectonic evolution of the Slovenian Periadriatic fault: Implications for Alpine-Carpathian extrusion models.– *Tectonics*, 17/5, 690–709. doi: 10.1029/98TC01605
- FOSTER, M.D. (1962): Interpretation of the composition and a classification of the chlorites.– *U.S. Geological Survey Professional Paper*, 414, 1–33.
- FRANZ, G., ANDREHS, G., & RHEDE, D. (1996): Crystal chemistry of monazite and xenotime from Saxothuringian-Moldanubian metapelites, NE Bavaria, Germany.– *Eur. J. Mineral.* 8, 1097–1118. doi: 10.1127/ejm/8/5/1097
- FRANCESCHELLI, M. & MEMMI, I. (1999): Zoning of chloritoid from kyanite-facies metapsammites, Alpi Apuane, Italy.– *Mineralogical Magazine*, 63/1, 105–110. doi: 10.1180/minmag.1999.063.1.10
- FUHRMAN, M.L. & LINDSLEY, D.H. (1988): Ternary-feldspar modelling and thermometry.– *Am. Mineral.*, 73, 201–215.
- HAAS, J., MIOČ, P., PAMIĆ, J., TOMLJENOVIC, B., ÁRKAI, P., BÉRCZI-MAKK, A. & RÁLISCH-FELGENHAUER, E. (2000): Complex structural pattern of the Alpine-Dinaridic-Pannonian triple junction.– *International Journal of Earth Sciences*, 89/2, 377–389. doi: 10.1007/s005310000093
- HEINRICH, W., ANDREHS, G., & FRANZ, G. (1997): Monazite-xenotime miscibility gap thermometry. I. An empirical calibration.– *J. Metamorph. Geol.*, 15, 3–16. doi: 10.1111/j.1525-1314.1997.t01-1-00052.x
- INOUE, A., INOUE, S. & UTADA, M. (2018): Application of chlorite thermometry to estimation of formation temperature and redox conditions.– *Clay Minerals*, 53, 143–158. doi: 10.1180/clm.2018.10
- JANOUŠEK, V., FARROW, C.M. & ERBAN, V. (2006): Interpretation of whole-rock geochemical data in igneous geochemistry: introducing Geochemical Data Toolkit (GCDkit).– *Journal of Petrology*, 47/6, 1255–1259. doi: 10.1093/petrology/egl013
- JUDIK, K., ÁRKAI, P., HORVÁTH, P., et al. (2004): Diagenesis and low-temperature metamorphism of Mt. Medvednica, Croatia: Mineral assemblages and phyllosilicate characteristics.– *Acta geologica Hungarica*, 47, 151–176. doi: 10.1556/AGeo.47.2004.2-3.5
- JUDIK, K., BALOGH, K., TIBLJAŠ, D. & ÁRKAI, P. (2006): New age data on the low-temperature regional metamorphism of Mt. Medvednica (Croatia).– *Acta geologica Hungarica*, 49, 207–221. doi: 10.1556/AGeo.49.2006.3.2
- JUDIK, K., RANTITSCH, G., RAINER, T.M., et al. (2008): Alpine metamorphism of organic matter in metasedimentary rocks from Mt. Medvednica (Croatia).– *Swiss Journal of Geosciences*, 101, 605–616. doi: 10.1007/s00015-008-1303-z
- KARAMATA, S. (2006): The geological development of the Balkan Peninsula related to the approach, collision and compression of Gondwana and Eurasian units.– In: ROBERTSON, AHF & MOUNTRAKIS, D. (eds.): *Tectonic development of the Eastern Mediterranean Region*.– Geological Society, London, Special Publications, 260, 155–178.
- KOROKNAY, B., HORVÁTH, P. & NÉMETH, T. (2001): Chloritoid schist from the Uppony Mts (NE Hungary): Mineralogical, petrological and structural data from a new occurrence.– *Acta Geologica Hungarica*, 44/1, 47–65.
- LANPHERE, M.A., COLEMAN, R.G., KARAMATA, S. & PAMIĆ, J. (1975): Age of amphibolites associated with alpine peridotites in the Dinaride ophiolite zone, Yugoslavia.– *Earth and Planetary Science Letters*, 26, 271–276. doi: 10.1016/0012-821X(75)90001-1
- LI, B., MASSONNE, H.-J., KOLLER, F. & ZHANG, J.-F. (2021): Metapelite from the high-ultrahigh pressure terrane of the Eastern Alps (Pohorje Mts., Slovenia) – new pressure, temperature, and time constraints on a polymetamorphic rock.– *Journal of Metamorphic Geology*, 39/6, 695–726. doi: 10.1111/jmg.12581
- LO PÒ, D. & BRAGA, R. (2014): Influence of ferric iron on phase equilibria in greenschist facies assemblages: The hematite-rich metasedimentary rocks from the Monti Pisanì (Northern Apennines).– *Journal of Metamorphic Geology*, 32, 371–387. doi: 10.1111/jmg.12076
- LUGOVÍC, B., ŠEGVIĆ, B. & ALATHERR, R. (2006): Petrology, geochemistry and tectonic significance of the orthogneisschists from the SW Zagorje-Mid-Transdanubian Zone (Medvednica Mts, Croatia).– *Ophioliti*, 31/1, 39–50.
- MASSONNE, H.-J. (2012): Formation of amphibole and clinozoisite-epidote in eclogite owing to fluid infiltration during exhumation in a subduction channel.– *Journal of Petrology*, 53, 1969–1998. doi: 10.1093/petrology/egs040
- MASSONNE, H.-J. (2014): Wealth of P-T-t information in medium-high grade metapelites: example from the Jubrique Unit of the Betic Cordillera, S. Spain.– *Lithos*, 208–209, 137–157. doi: 10.1016/j.lithos.2014.08.027
- MASSONNE, H.-J. & SCHREYER, W. (1989): Stability field of the high-pressure assemblage talc + phengite and two new phengite barometers.– *European Journal of Mineralogy*, 1, 391–410. doi: 10.1127/ejm/1/3/0391
- MASSONNE, H.-J. & SZPURKA, Z. (1997): Thermodynamic properties of white micas on the basis of high-pressure experiments in the systems $\text{K}_2\text{O}-\text{MgO}-\text{Al}_2\text{O}_3-\text{SiO}_2-\text{H}_2\text{O}$ and $\text{K}_2\text{O}-\text{FeO}-\text{Al}_2\text{O}_3-\text{SiO}_2-\text{H}_2\text{O}$.– *Lithos*, 41, 229–250. doi: 10.1016/S0024-4937(97)82014-2
- MASSONNE, H.-J., DRISTAS, J.A. & MARTÍNEZ, J.C. (2012): Metamorphic evolution of the Río de la Plata craton in the Cinco Cerros area, Buenos Aires Province, Argentina.– *Journal of South American Earth Sciences*, 38, 57–70. doi: 10.1016/j.jsames.2012.05.005
- MCLENNAN, S.M., (2001): Relationships between the trace element composition of sedimentary rocks and upper continental crust.– *Geochemistry Geophysics Geosystems*, 2, 1021. doi: 10.1029/2000GC000109
- MCLENNAN, S.M. & TAYLOR, S.R. (1991): Sedimentary rocks and crustal evolution: tectonic setting and secular trends.– *J. Geol.*, 99, 1–21. doi: 10.1086/629470
- MIŠUR, I. (2017): Geodinamska evolucija metasedimentnih stijena niskog stupnja metamorfizma na Medvednici [Geodynamic evolution of low grade metasedimentary rocks on the Mt. Medvednica.– in Croatian, with an English Abstract].– Unpubl. PhD Thesis, Faculty of Science, University of Zagreb, 215 p.
- MIŠUR, I., BELAK, M. & BALEN, D. (2013): Petrographic features of chloritoid schist from southeastern slopes of Mt. Medvednica, (Zagorje-Mid-Transdanubian zone, Croatia).– In: SCHUSTER, R. (ed.): 11th Workshop on Alpine Geological Studies and 7th European Symposium on Fossil Algae, Abstracts & Field Guides. Wien, Geologische Bundesanstalt, 66–67.
- MIŠUR, I., BELAK, M., KLÖTZLI, U. & BALEN, D. (2015): Evidence from chloritoid schists for multi-stage metamorphism in the Mt. Medvednica area (Zagorje Mid Transdanubian zone, N Croatia).– In: KOLLER, F., KOLITSCH, U. & TESSADRI, R. (eds.): MinPet2015, Mitteilungen Österreichischen Minerologischen Gesellschaft, 161, 89–89.
- MONTEL, J., FORET, S., VESCHAMBRE, M., NICOLLET, C. & PROVOST, A. (1996): Electron microprobe dating of monazite.– *Chemical Geology*, 131, 37–53. doi: 10.1016/0009-2541(96)00024-1
- MPOSKOS, E. (1989): High-pressure metamorphism in gneisses and pelitic schists in the East Rhodope zone (N. Greece).– *Mineralogy and Petrology*, 41, 25–39. doi: 10.1007/bf01164808
- OKRUSCH, M., SEIDEL, E., KREUZER, H. & HARRE, W. (1978): Jurassic age of metamorphism at the base of the Brezovica peridotite (Yugoslavia).– *Earth and Planetary Science Letters*, 39, 291–297. doi: 10.1016/0012-821X(78)90205-4
- ONDREJKA, M., UHER, P., PUTIŠ, M., BROSKA, I., BAČÍK, P., KONEČNÝ, P. & SCHMIEDT, I. (2012): Two stage breakdown of monazite by post-magmatic and metamorphic fluids: an example from the Veporic orthogneiss, Western Carpathians, Slovakia.– *Lithos* 142–143, 245–255. doi: 10.1016/j.lithos.2012.03.012
- PAMIĆ, J. (1984): Triassic magmatism of the Dinarides in Yugoslavia.– *Tectonophysics*, 109/3–4, 273–307.
- PAMIĆ, J. (2002): The Sava-Vardar Zone of the Dinarides and Hellenides versus the Vardar Ocean.– *Eclogae Geologicae Helvetiae*, 95, 99–113.

- PAMIĆ, J. & TOMLJENOVIC, B. (1998): Basic geological data from the Croatian part of the Zagorje-Mid-Transdanubian zone.– *Acta Geologica Hungarica*, 41(4), 389–400.
- PARRISH, R.R. (1990): U-Pb dating of monazite and its application to geological problems.– *Canadian Journal of Earth Sciences*, 27, 1431–1450. doi: 10.1139/c90-152
- PARRY, W.T., BALLANTYNE, J.M. & JACOBS, D.C. (1984): Geochemistry of hydrothermal sericite from Roosevelt Hot Springs and the Tintic and Santa Rita porphyry copper systems.– *Econ. Geol.* 79, 72–86. doi: 10.2113/gsecongeo.79.1.72.
- PASSCHIER, C.W. & TROUW, R.A.J. (2005): *Microtectonics*.– Heidelberg, Springer-Verlag Berlin, 366 p. doi: 10.1007/978-3-662-08734-3
- PORKOLÁB, K., DURETZ, T., YAMATO, P., AUZEMERY, A. & WILLINGSHOFER, E. (2021): Extrusion of subducted crust explains the emplacement of far-travelled ophiolites.– *Nature Communications*, 12, 1499. doi: 10.1038/s41467-021-21866-1
- POUCHOU, J.L. & PICHOIR, F. (1984): A new model for quantitative analysis: Part I. Application to the analysis of homogeneous samples.– *LaRecherche Aerospatiale*, 3, 13–38.
- POUCHOU, J.L. & PICHOIR, F. (1991): Quantitative analysis of homogeneous or stratified microvolumes applying the model "PAP".– In: HEINRICH, K.F.J. & NEWBURY, D.E. (ed), *Electron Probe Quantitation*, Plenum, New York, 31–75. doi: 10.1007/978-1-4899-2617-3_4
- PYLE, J.M., SPEAR, F.S., RUDNICK, R.L. & MCDONOUGH, W.F. (2001): Monazite–xenotime–garnet equilibria in metapelites and a new monazite–garnet thermometer.– *Journal of Petrology*, 42, 2083–2107. doi: 10.1093/petrology/42.11.2083
- ROBERTSON, A (2004): Development of concepts concerning the genesis and emplacement of Tethyan ophiolites in the Eastern Mediterranean and Oman regions.– *Earth-Science Reviews*, 66, 331–387. doi: 10.1016/j.earscirev.2004.01.005
- SCHEFER, S., EGLI, D., MISSONI, S., BERNOULLI, D., FÜGENSCHUH, B., GAWLIK, H.-J., JOVANOVIĆ, D., KRYSZTYN, L., LEIN, R., SCHMID, S.M. & SU-DAR, M.N. (2010): Triassic metasediments in the internal Dinarides (Kopaonik area, southern Serbia): stratigraphy, Palaeogeographic and tectonic significance.– *Geologica Carpathica* 61, 89–109. doi: 10.2478/v10096-010-0003-6
- SCHMID, S.M., BERNOULLI, D., FÜGENSCHUH, B., MATENCO, L., SCHEFER, S., SCHUSTER, R., TISCHLER, M. & USTASZEWSKI, K. (2008): The Alpine-Carpathian-Dinaridic orogenic system: Correlation and evolution of tectonic units.– *Swiss Journal of Geosciences*, 101, 139–183. doi: 10.1007/s00015-008-1247-3
- SCHMID, S.M., BERNOULLI, D., FÜGENSCHUH, B., GEORGIEV, N., KOUNOV, A., MATENCO, L., OBERHÄNSLI, R., PLEUGER, J., SCHEFER, S., USTASZEWSKI, K. & VAN HINSBERGEN, D. (2016): Map of the Tectonic units of the Alpine collision zone between Eastern Alps and Western Turkey. <https://www.researchgate.net/publication/292606123>
- SCHMID, S.M., FÜGENSCHUH, B., KOUNOV, A., MATENCO, L., NIEVERGELT, P., OBERHÄNSLI, R., PLEUGER, J., SCHEFER, S., SCHUSTER, R., TOMLJENOVIC, B., USTASZEWSKI, K. & VAN HINSBERGEN, D.J.J. (2020): Tectonic units of the Alpine collision zone between Eastern Alps and Western Turkey.– *Gondwana Research*, 78, 308–374. doi: 10.1016/j.gr.2019.07.005
- SCHULZ, B. (2021): Monazite Microstructures and Their Interpretation in Petrochronology.– *Frontiers in Earth Science*, 9, 668566. doi: 10.3389/feart.2021.668566
- SLOVENEC, D., ŠEGVIĆ, B. & VLAHOVIĆ, I. (2010): Geochemistry, petrology and tectonomagmatic significance of basaltic rocks from the ophiolite mélange at the NW External-Internal Dinarides junction (Croatia).– *Geologica Carpathica*, 61, 4, 273–292. doi: 10.2478/v10096-010-0016-1
- SLOVENEC, D., ŠEGVIĆ, B., HALAMIĆ, J., GORIĆAN, Š. & ZANONI, G. (2020): An ensialic volcanic arc along the northwestern edge of Palaeotethys—Insights from the Mid-Triassic volcanosedimentary succession of Ivanščica Mt. (northwestern Croatia).– *Geological Journal*, 55, 4324–4351. doi: 10.1002/gj.3664
- SPEAR, F.S. (1995): Metamorphic Phase Equilibria and Pressure-Temperature-Time Paths. Monograph 1 (2nd reprinted edition).– Mineralogical Society of America, Chantilly, Virginia, 799.
- SPEAR, F. S. & PYLE, J. M. (2002): Apatite, monazite and xenotime in metamorphic rocks.– *Rev. Mineral. Geochem.* 48, 293–335. doi: 10.1515/9781501509636-010
- STIPP, M., STÜNITZ, H., HEILBRONNER, R. & SCHMID, S. M. (2002): Dynamic recrystallisation of quartz: Correlation between natural and experimental conditions.– In: S. De MEER et al. (eds.): *Deformation Mechanisms, Rheology and Tectonics: Current Status and Future Perspectives*. *Geol. Soc. Spec. Publ.*, 200, 171 – 190.
- SUZUKI, K & KATO, T (2008): CHIME dating of monazite, xenotime, zircon and polycrase: Protocol, pitfalls and chemical criterion of possibly discordant age data.– *Gondwana Research*, 14, 569–586. doi: 10.1016/j.gr.2008.01.005
- ŠEGVIĆ, B., KUKOĆ, D., DRAGIČEVIĆ, I., VRANJKOVIĆ, A., BRČIĆ, V., GORIĆAN, Š., BABAJIĆ, E. & HRVATOVICIĆ, H. (2014): New record of Middle Jurassic radiolarians and evidence of Neotethyan dynamics documented in a mélange from the Central Dinaridic Ophiolite Belt (CDOB, NE Bosnia and Herzegovina).– *Ophioliti*, 39, 33–43. doi:10.4454/opholiti.v39i1.427
- ŠEGVIĆ, B., SLOVENEC, D., ALTHERR, R., BABAJIĆ, E., MÄHLMANN, R.F. & LUGOVIĆ, B. (2019): Petrogenesis of high-grade metamorphic soles from the Central Dinaric Ophiolite belt and their significance for the Neotethyan evolution in the Dinarides.– *Ophioliti*, 44, 1–30. doi:10.4454/opholiti.v44i1.462
- ŠEGVIĆ, B., SLOVENEC, D., SCHUSTER, R., BABAJIĆ, E., BADURINA, L. & LUGOVIĆ, B. (2020): Sm-Nd geochronology and petrologic investigation of a sub-ophiolitic metamorphic sole from the Dinarides (Krivaja-Konjuh Ophiolite Complex, Bosnia and Herzegovina).– *Geologija Croatica*, 73/2, 119–130. doi: 10.4154/gc.2020.09
- ŠIKIĆ, K., BASCH, O. & ŠIMUNIĆ, A. (1978): Osnovna geološka karta SFRJ, list Zagreb 1:100.000 L 33-80 [Basic Geological Map of SFRY 1:100000, Zagreb sheet – in Croatian].– Institut za geološka istraživanja, Zagreb, Savezni geološki zavod Beograd.
- ŠIKIĆ, K., BASCH, O. & ŠIMUNIĆ, A. (1979): Tumač osnovne geološke karte SFRJ 1:100.000 L 33-80, list Zagreb [Basic Geological Map of SFRY 1:100000, Geology of the Zagreb sheet – in Croatian].– Institut za geološka istraživanja, Zagreb, Savezni geološki zavod Beograd.
- TAYLOR, S.R. & MCLENNAN, S.M. (1995): The geochemical evolution of the continental crust.– *Reviews of Geophysics*, 33/2, 241–265. doi: 10.1029/95RG00262
- TISCHENDORF, G., FÖRSTER, H.J., GOTTESMANN, B., RIEDER, M., (2007): True and brittle micas: composition and solid-solution series.– *Mineralogical Magazine*, 71/3, 285–320. doi: 10.1180/minmag.2007.071.3.285
- TOLJIĆ, M., MATENCO, L., DUCEA, M.N., STOJADINOVIC, U., MILIVOJEVIĆ, J. & ĐERIĆ, N. (2013): The evolution of a key segment in the Europe-Adria collision: The Fruška Gora of northern Serbia.– *Global Planet. Change*, 103, 39–62. doi: 10.1016/j.gloplacha.2012.10.009
- TOMLJENOVIC, B. (2002): Strukturne značajke Medvednice i Samoborskog gorja [Structural Characteristics of Medvednica and Samoborsko Gorje Mountains – in Croatian with an English Abstract].– Unpubl. PhD Thesis, Faculty of Science, University of Zagreb, Faculty of Mining, Geology and Petroleum engineering. 208 p.
- TOMLJENOVIC, B., CSONTOS, L., MÁRTON, E. & MÁRTON, P. (2008): Tectonic evolution of the northwestern Internal Dinarides as constrained by structures and rotation of Medvednica Mountains, North Croatia.– *Geological Society London, Special Publications*, 298, 145–167. doi: 10.1144/SP298.8
- USTASZEWSKI, K., SCHMID, S.M., FÜGENSCHUH, B., TISCHLER, M., KISSLING, E. & SPAKMAN, W. (2008): A map-view restoration of the Alpine-Carpathian-Dinaridic system for the Early Miocene.– *Swiss Journal of Geosciences*, 101/1, 273–294. doi: 10.1007/s00015-008-1288-7
- USTASZEWSKI, K., SCHMID, S.M., LUGOVIĆ, B., SCHUSTER, R., SCHALTEGGER, U., BERNOULLI, D., HOTTINGER, L., KOUNOV, A., FÜGENSCHUH, B. & SCHEFER, S. (2009): Late Cretaceous intra-oceanic magmatism in the Internal Dinarides (northern Bosnia and Herzegovina): Implications for the collision of the Adriatic and European plates.– *Lithos*, 108/1–4, 106–125. doi: 10.1016/j.lithos.2008.09.010
- VAN GELDER, I.E., MATENCO, L., WILLINGSHOFER, E., TOMLJENOVIC, B., ANDRIESSEN, P.A.M., DUCEA, M.N. & GRUIĆ, A. (2015): The tectonic evolution of a critical segment of the Dinarides-Alps connection: Kinematic and geochronological inferences from the Medvednica Mountains, NE Croatia.– *Tectonics* 34/9, 1952–1978. doi: 10.1002/2015TC003937
- VERMEESCH, P. (2018): IsoplotsR: a free and open toolbox for geochronology.– *Geoscience Frontiers*, v.9, 1479–1493. doi: 10.1016/j.gsf.2018.04.001
- VERNON, R. H. (2004): A practical guide to rock microstructure.– Cambridge University Press, Cambridge, 594. doi: 10.1017/CBO9780511807206
- VIDAL, O., GOFFÉ, B., BOUSQUET, R. & PARRA, T. (1999): Calibration and testing of an empirical chloritoid-chlorite Mg-Fe exchange thermometer and thermodynamic data for daphnite.– *Journal of Metamorphic Geology*, 17, 25–39. doi: 10.1046/j.1525-1314.1999.00174.x
- VIDAL, O., LANARI, P., MUÑOZ, M., BOURDELLE, F. & DE ANDRADE, V. (2016): Deciphering temperature, pressure, and oxygen activity conditions of chlorite formation.– *Clay Minerals*, 51, 615–633. doi: 10.1180/claymin.2016.051.4.06
- VRAGOVIĆ, M. & MAJER, V. (1979a): Kloritoidni škriljevi u metamorfnim kompleksima u sjevernoj Hrvatskoj (Jugoslavija) [Chloritoid schists in metamorphic complexes in northern Croatia (Yugoslavia)(in Croatian)].– *Geološki vjesnik*, 31, 287–294
- VRAGOVIĆ, M. & MAJER, V. (1979b): Prilozi za poznavanje metamorfnih stijena Zagrebačke gore, Moslavačke gore i Papuka (Hrvatska, Jugoslavija)[Contributions to the knowledge of metamorphic rocks of Zagrebačka Mt., Moslavačka Mt. and Papuk Mt. (Croatia, Yugoslavia)(in Croatian)].– *Geol. vjesnik*, 31, 295–308.
- WILLIAMS, M., JERCINOVIC, M.J. & HETHERINGTON, C.J. (2007): Microprobe monazite geochronology: understanding geologic processes by integrating composition and chronology.– *Annual Review of Earth and Planetary Sciences*, 35, 137–175. doi: 10.1146/annurev.earth.35.031306.140228
- WHITE, R.W., POWELL, R., HOLLAND, J.B., JOHNSON, T.E. & GREEN, E.C.R. (2014): New mineral activity-composition relations for thermodynamic calculations in metapelitic systems.– *Journal of Metamorphic Geology*, 32, 261–286. doi: 10.1111/jmg.12071
- ZANE, A. & WEISS, Z. (1998): A procedure for classifying rock-forming chlorites based on microprobe data.– *Rendiconti Lincei*, 9, 51–56. doi: 10.1007/BF02904455

Supplementary data



Supplement 1. Pseudosection calculated in the system MnNCKFMASHTO with various (0%, 5%, 15%, 20%) percentages of ferric iron in the bulk-rock composition of sample ST-6, (MnNCKFMASHTO = MnO-Na₂O-CaO-K₂O-FeO-MgO-Al₂O₃-SiO₂-H₂O-TiO₂-O₂) using the PERPLE_X software package (CONNOLLY & PETRINI, 2002; CONNOLY, 1990; 2005). The numbers in the circles refer to mineral assemblages given at the bottom. Abbreviations: and –andalusite; Bio –biotite; Ca –carpholite; Chl –chlorite; Ctd –chloritoid; Gt –garnet; Ilm –ilmenite; Mica –muscovite; St –staurolite; ru –rutile; Q –quartz. The coloured lines in the diagrams refer to isopleths of chloritoid (red), muscovite (blue), and chlorite (yellow).